Atmos. Chem. Phys., 14, 5807–5824, 2014
www.atmos-chem-phys.net/14/5807/2014/
doi:10.5194/acp-14-5807-2014

Atmospheric Chemistry and Physics
Open Access

Estimating Asian terrestrial carbon fluxes from CONTRAIL aircraft and surface CO_2 observations for the period 2006–2010

H. F. Zhang[1,2], B. Z. Chen[1], I. T. van der Laan-Luijkx[3], T. Machida[4], H. Matsueda[5], Y. Sawa[5], Y. Fukuyama[6], R. Langenfelds[7], M. van der Schoot[7], G. Xu[1,2], J. W. Yan[1,2], M. L. Cheng[1,2], L. X. Zhou[8], P. P. Tans[9], and W. Peters[3,10]

[1]State Key Laboratory of Resources and Environment Information System, Institute of Geographic Sciences and Natural Resources Research, Chinese Academy of Sciences, Beijing 100101, China
[2]University of Chinese Academy of Sciences, Beijing 100049, China
[3]Department of Meteorology and Air Quality (MAQ), Wageningen University, Droevendaalsesteeg 3a, 6700 PB, Wageningen, the Netherlands
[4]Center for Global Environmental Research, National Institute for Environmental Studies, Tsukuba, Japan
[5]Geochemical Research Department, Meteorological Research Institute, Tsukuba, Japan
[6]Atmospheric Environment Division, Global Environment and Marine Department, Japan Meteorological Agency, Japan
[7]Centre for Australian Weather and Climate Research/CSIRO Marine and Atmospheric Research, Aspendale, Victoria, Australia
[8]Key Laboratory for Atmospheric Chemistry of China Meteorological Administration, Research Institute of Atmospheric Composition of Chinese Academy of Meteorological Sciences, Beijing 100081, China
[9]Earth System Research Laboratory, National Oceanographic and Atmospheric Administration, Boulder, Colorado 80305, USA
[10]Centre for Isotope Research, Groningen, the Netherlands

Correspondence to: B. Z. Chen (baozhang.chen@igsnrr.ac.cn) and W. Peters (wouter.peters@wur.nl)

Received: 9 October 2013 – Published in Atmos. Chem. Phys. Discuss.: 24 October 2013
Revised: 16 April 2014 – Accepted: 25 April 2014 – Published: 11 June 2014

Abstract. Current estimates of the terrestrial carbon fluxes in Asia show large uncertainties particularly in the boreal and mid-latitudes and in China. In this paper, we present an updated carbon flux estimate for Asia ("Asia" refers to lands as far west as the Urals and is divided into boreal Eurasia, temperate Eurasia and tropical Asia based on TransCom regions) by introducing aircraft CO_2 measurements from the CONTRAIL (Comprehensive Observation Network for Trace gases by Airline) program into an inversion modeling system based on the CarbonTracker framework. We estimated the averaged annual total Asian terrestrial land CO_2 sink was about $-1.56\,\mathrm{Pg\,C\,yr^{-1}}$ over the period 2006–2010, which offsets about one-third of the fossil fuel emission from Asia ($+4.15\,\mathrm{Pg\,C\,yr^{-1}}$). The uncertainty of the terrestrial uptake estimate was derived from a set of sensitivity tests and ranged from -1.07 to $-1.80\,\mathrm{Pg\,C\,yr^{-1}}$, comparable to the formal Gaussian error of $\pm 1.18\,\mathrm{Pg\,C\,yr^{-1}}$ (1-sigma). The largest sink was found in forests, predominantly in coniferous forests ($-0.64 \pm 0.70\,\mathrm{Pg\,C\,yr^{-1}}$) and mixed forests ($-0.14 \pm 0.27\,\mathrm{Pg\,C\,yr^{-1}}$); and the second and third large carbon sinks were found in grass/shrub lands and croplands, accounting for $-0.44 \pm 0.48\,\mathrm{Pg\,C\,yr^{-1}}$ and $-0.20 \pm 0.48\,\mathrm{Pg\,C\,yr^{-1}}$, respectively. The carbon fluxes per ecosystem type have large a priori Gaussian uncertainties, and the reduction of uncertainty based on assimilation of sparse observations over Asia is modest (8.7–25.5 %) for most individual ecosystems. The ecosystem flux adjustments follow the detailed a priori spatial patterns by design, which further increases the reliance on the a priori biosphere exchange model. The peak-to-peak amplitude of inter-annual variability (IAV) was $0.57\,\mathrm{Pg\,C\,yr^{-1}}$ ranging from $-1.71\,\mathrm{Pg\,C\,yr^{-1}}$ to $-2.28\,\mathrm{Pg\,C\,yr^{-1}}$. The IAV analysis reveals that the Asian CO_2 sink was sensitive to climate variations, with the lowest uptake in 2010 concurrent with a summer flood and autumn drought and the largest CO_2 sink in 2009 owing to favorable temperature and plentiful

precipitation conditions. We also found the inclusion of the CONTRAIL data in the inversion modeling system reduced the uncertainty by 11 % over the whole Asian region, with a large reduction in the southeast of boreal Eurasia, southeast of temperate Eurasia and most tropical Asian areas.

1 Introduction

The concentration of carbon dioxide (CO_2) has been increasing steadily in the atmosphere since the industrial revolution, which is considered very likely to be responsible for the largest contribution of the climate warming (Huber and Knutti, 2011; Peters et al., 2011). Knowledge of the terrestrial carbon sources and sinks is critically important for understanding and projecting the future atmospheric CO_2 levels and climate change. The global terrestrial ecosystems absorbed about 1–3 Pg carbon every year during the 2000s, with obvious interannual variations, offsetting 10–40 % of the anthropogenic emissions (Le Quéré et al., 2009; Maki et al., 2010; Saeki et al., 2013). However, estimates of the terrestrial carbon balance vary considerably when considering continental scales and smaller, as well as when estimating the CO_2 seasonal and inter-annual variability (Houghton, 2007; Peylin et al., 2013).

Asia, as one of the biggest Northern Hemisphere terrestrial carbon sinks, has a significant impact on the global carbon budget (Jiang et al., 2013; Patra et al., 2012; Piao et al., 2009, 2012; Peylin et al., 2013; Yu et al., 2013). It is estimated that Asian ecosystems contribute over 50 % of the global net terrestrial ecosystem exchange (Maksyutov et al., 2003) and their future balance is thought to be a great source of uncertainty in the global carbon budget (Ichii et al., 2013; Oikawa and Ito, 2001). Even though the importance of the Asian ecosystems is increasingly recognized and many efforts have been carried out to estimate the Asian terrestrial carbon sources and sinks, they still remain poorly quantified (Ito, 2008; Patra et al., 2012, 2013; Piao et al., 2011). One reason is that a steep rise of fossil fuel emissions in most Asian countries has imposed large influences on the Asian CO_2 balance and leads to an increased variability of the regional carbon cycle (Francey et al., 2013; Le Quere et al., 2009; Patra et al., 2011, 2013; Raupach et al., 2007). In addition, rapid land-use change and climate change have likely increased the variability in the Asian terrestrial carbon balance (Cao et al., 2003; Patra et al., 2011; Yu et al., 2013). This makes it challenging to accurately estimate CO_2 fluxes of the Asia ecosystems.

Currently two approaches are commonly used to estimate CO_2 fluxes at regional to global scales: the so-called "bottom-up" and "top-down" methods. The bottom-up approach is based on local data or field measurements to retrieve the carbon fluxes, including direct measurements (Chen et al., 2012; Clark et al., 2001; Fang et al., 2001; Mizoguchi et al., 2009; Takahashi et al., 1999) and ecosystem modeling (Chen et al., 2007; Fan et al., 2012; Randall et al., 1996; Randerson et al., 1997; Sellers et al., 1986, 1996). The top-down method uses atmospheric mole fraction data to derive the CO_2 sink/source information. As one of the important "top-down" approaches, atmospheric inverse modeling has been well developed and widely applied (Baker et al., 2006; Chevallier and O'Dell, 2013; Deng et al., 2007; Gurney et al., 2003; Gurney et al., 2004), and has shown to be particularly successful in estimating regional carbon flux for regions rich in atmospheric CO_2 observations like North America and Europe (Broquet et al., 2013; Deng et al., 2007; Peters et al., 2007, 2010; Peylin et al., 2005, 2013; Rivier et al., 2011, 2010). However, estimating Asian CO_2 surface fluxes with inverse modeling remains challenging, and the inverted Asian CO_2 fluxes still exhibit a large uncertainty partly because of a lack of surface CO_2 observations. For example, in the TransCom3 annual mean control inversion, Gurney et al. (2003) used a set of 17 models to estimate the carbon fluxes and obtained different results for the Asian biospheric CO_2 budget, ranging from a large CO_2 source of $+1.00 \pm 0.61$ Pg C yr^{-1} to a large sink of -1.50 ± 0.67 Pg C yr^{-1} for the year 1992–1996. In the RECCAP (REgional Carbon Cycle Assessment and Processes) project, Piao et al. (2012) presented the carbon balance of terrestrial ecosystems in East Asia from eight inversions during the period 1990–2009. The results from these eight inversion models also show disagreement. Six models estimate a net CO_2 uptake with the highest net carbon sink of -0.997 Pg C yr^{-1}, while two models show a net CO_2 source with the largest net carbon emission of $+0.416$ Pg C yr^{-1} in East Asia. The important role of the sparse observational network was demonstrated by Maki et al. (2010), who reported a large Asian land sink of -1.17 ± 0.50 Pg C yr^{-1} or much smaller sink of -0.65 ± 0.49 Pg C yr^{-1} over the Asian region depending on which set of observations was included in the same inversion system. This situation suggests that a more accurate estimate of the surface CO_2 flux is urgently required in Asia, and the ability to base it on as much observational data as possible is key.

To expand the number of CO_2 observations, the aircraft project CONTRAIL has measured CO_2 mole fractions onboard passenger flights since 2005, and has produced a large coverage of in situ CO_2 data ranging over various latitudes, longitudes, and altitudes (Machida et al., 2008; Matsueda et al., 2008). CONTRAIL observations have also already successfully been used to constrain surface flux estimates (Niwa et al., 2011, 2012; Patra et al., 2011). Patra et al. (2011) reported the added value of CONTRAIL data to inform on tropical Asian carbon fluxes, as their signals are transported rapidly to the free troposphere over the west Pacific.

In this study, we also used the CONTRAIL CO_2 observations (http://www.cger.nies.go.jp/contrail/) together with a global network of surface observations to estimate the Asian weekly net ecosystem exchange of CO_2 (NEE) during the

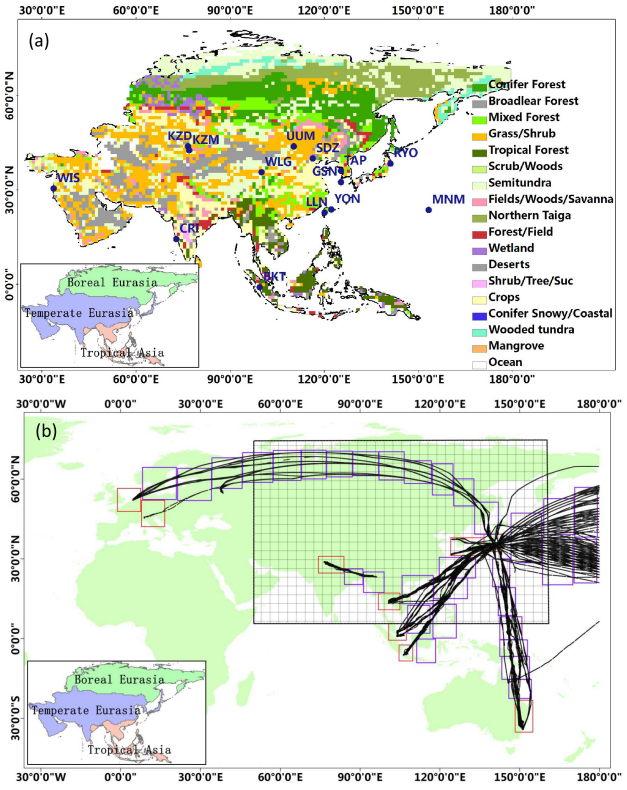

Figure 1. (a) Map of the Asian surface observation sites, along with the map of the ecoregion types from Olson et al. (1985) with 19 land cover classes as used in this study. These Asian surface observation data download from the NOAA-ESRL (e.g., Mt. Waliguan, China (WLG), Bukit Kototabang, Indonesia (BKT), Sede Boker, Israel (WIS), Sary Taukum, Kazakhstan (KZD), Plateau Assy, Kazakhstan (KZM), Tae-ahn Peninsula,South Korea (TAP), Ulaan Uul, Mongolia (UUM), Cape Rama, India (CRI)) and WDCGG network (e.g., Lulin, Taiwan (LLN), Shangdianzi, China (SDZ), Minamitorishima, Japan (MNM), Ryori, Japan (RYO), Yonagunijima, Japan (YON), Gosan, South Korea (GSN)); **(b)** CONTRAIL CO_2 observations map, along with 42 horizontal regions. The red rectangles represent the nine regions covering the ascending and descending data (included four vertical bins at 575–625, 475–525, 375–425, 225–275 hPa) over airports, and the blue rectangles indicate the other 33 regions covering the cruise data (included one bin at 225–275 hPa). The big black rectangle indicates a zoom region over Asia ($1^\circ \times 1^\circ$) based on global grid ($3^\circ \times 2^\circ$). Note that "Asia" refers to lands as far west as the Urals in this study and it is further divided into boreal Eurasia, temperate Eurasia and tropical Asia based on TransCom regions (Gurney et al., 2002; Gurney et al., 2003). These divided regions are presented in the small inset in the bottom left corner (same as thereafter).

period 2006–2010. Our inversion model is the state-of-the-art CO_2 data assimilation system CTDAS (CarbonTracker Data Assimilation Shell, http://carbontracker.eu/ctdas/). Our work complements previous inverse modeling studies as it (1) presents the inverted CO_2 results of Asian weekly net ecosystem exchange not shown previously; (2) uses surface observations not available in earlier top-down estimates; (3) assimilates the continuous CO_2 observation from a number of Asian continental sites for the first time; (4) includes extra free tropospheric CO_2 observations to further constrain the estimate; (5) uses a two-way atmospheric transport model TM5 (Krol et al., 2005) with higher horizontal resolution than previous global CO_2 data assimilation studies that focused on Asia (this study uses a $1^\circ \times 1^\circ$ grid over Asia while globally a $2 \times 3^\circ$ resolution, see Fig. 1b).

This paper is organized as follows. Methods and materials are described in Sect. 2, the inferred Asian land flux and its temporal-spatial variations are presented in Sect. 3. To examine the impact of CONTRAIL data on Asian flux estimates, we also compared inverse results with and without CONTRAIL data during the period 2006–2010. In Sect. 4, we compare our inverted Asian surface fluxes with previous findings and discuss our uncertainty estimates and future directions. Note that "Asia" refers to lands as far west as the Urals, and it is further divided into boreal Eurasia, temperate Eurasia and tropical Asia based on TransCom regions (Gurney et al., 2002, 2003) (see small inset in the bottom left corner of Fig. 1).

2 Methods and data sets

2.1 The atmospheric inversion model (CTDAS)

The atmospheric inverse model CTDAS was developed by NOAA-ESRL (National Oceanic and Atmospheric Administration's Earth System Research Laboratory) and Wageningen University, the Netherlands. Previous versions of the system have been applied successfully in North America and Europe (Masarie et al., 2011; Peters et al., 2007, 2010). CTDAS was designed to estimate net CO_2 terrestrial and oceanic surface fluxes by integrating atmospheric CO_2 concentration measurements, a global transport model, and a Bayesian synthesis technique that minimizes the difference between the simulated and observed CO_2 concentrations. The first step is the forecast of the atmospheric CO_2 concentrations using the transport model TM5 (Krol et al., 2005) with a global resolution of $3^\circ \times 2^\circ$ and $1^\circ \times 1^\circ$ over Asia (Fig. 1b). The TM5 transport model is driven by meteorological data of the ERA-interim analysis of the European Centre for Medium-Range Weather Forecasts (ECMWF), and propagates four separate sets of bottom-up fluxes (details are presented in Sect. 2.2). The forecasted four-dimensional (4-D) concentrations (x, y, z, t) are sampled at the location and time of the observed atmospheric CO_2 mole fractions, and subsequently compared. The difference between the observed and simulated CO_2 concentrations is minimized. This minimization of the mole fraction differences in CTDAS is done by tuning a set of linear scaling factors which are applied to find the set of sources and sinks that most closely match the observed CO_2 concentration in the atmosphere.

As described in Peters et al. (2007), four a priori and imposed CO_2 fluxes integrate in CTDAS to instantaneous CO_2 fluxes $F(x, y, t)$ as follows:

$$F(x,y,t) = \lambda_r F_{\text{bio}}(x,y,t) + \lambda_r F_{\text{oce}}(x,y,t) + F_{\text{ff}}(x,y,t) + F_{\text{fire}}(x,y,t), \quad (1)$$

where F_{bio} and F_{oce} are 3-hourly, $1^\circ \times 1^\circ$ a priori terrestrial biosphere and ocean fluxes, respectively; F_{ff} and F_{fire} are monthly $1^\circ \times 1^\circ$ prescribed fossil fuel and fire emissions, and λ_r is a set of weekly scaling factors, and each scaling factor is associated with a particular region of the global domain that is divided into 11 land and 30 ocean regions according to climate zone and continent. Nineteen ecosystem types (Olson et al., 1985) (Fig. 1a) have been considered in each of the 11 global land areas (Gurney et al., 2002), dividing the globe into 239 regions ($239 = 11$ land $\times$ 19 ecosystem types $+ 30$ ocean regions). The actual region number assimilated in this system is 156, after excluding 83 regions which are associated with a non-existing ecosystem (such as "snowy conifers" in Africa). The corresponding scaling factors have been estimated as the final product of CTDAS, and have been applied to obtain the terrestrial biosphere and ocean fluxes at the ecosystem and ocean basin scale by multiplying them with the a priori fluxes. The adjusted fluxes are then put into the transport model to produce an optimized 4-D CO_2 mole fraction distribution.

2.2 A priori CO_2 flux data set

In CTDAS, four types of CO_2 surface fluxes are considered as follows: (1) the a priori estimates of the oceanic CO_2 exchange are based on the air–sea CO_2 partial pressure differences from ocean inversions results (Jacobson et al., 2007). These air–sea partial pressure differences are combined with a gas transfer velocity computed from wind speeds in the atmospheric transport model to compute fluxes of carbon dioxide across the sea surface every 3 h; (2) the a priori terrestrial biosphere CO_2 fluxes are from GFED2 (Global Fire Emissions Database version 2), which is derived from the Carnegie–Ames Stanford Approach (CASA) biogeochemical modeling system (Van der Werf et al., 2006). A monthly varying NEE flux ($\text{NEE} = R_e -$ GPP) was constructed from the following two flux components: gross primary production (GPP) and ecosystem respiration (R_e), and interpolated to 3-hourly net land surface fluxes using a simple temperature Q_{10} relationship assuming a global Q_{10} value of 1.5 for respiration, and a linear scaling of photosynthesis with solar radiation. (3) The imposed fossil fuel emission estimates from the global total fossil fuel emission of the CDIAC (Carbon Dioxide Information and Analysis Center) (Marland et al., 2003) were spatially and temporally interpolated following the EDGAR (Emission Database for Global Atmospheric Research) database (Boden et al., 2011; Commission, 2009; Olivier and Berdowski, 2001; Thoning et al., 1989); (4) the biomass-burning emissions are from GFED2, which combines monthly burned area information observed from satellites (Giglio et al., 2006) with the CASA biogeochemical model. Fire emissions in GFED2 are available only up to 2008, so for 2009 and 2010 we use a climatology of monthly averages of the previous decade. Note that GFED3 (and now even GFED4) is available for quite a few years, and offers higher spatial resolutions in biomass-burning emissions that are attractive for model simulation. But it uses a different product for the satellite observed NDVI (Normalized Difference Vegetation Index) and FPAR (the Fraction of Photosynthetically Active Radiation) (MODIS (the MODerate resolution Imaging Spectroradiometer) instead of AVHRR (Advanced Very High Resolution Radiometer)) which causes a different seasonality in the biosphere fluxes which are calculated alongside the fire emissions in GFED, with a less realistic amplitude. Since this amplitude of the seasonal biosphere is important to us, we did not update to this new GFED3 product. We also tested the GFED4 data with SIBCASA (Simple Biosphere/Carnegie-Ames-Stanford Approach) to make a new data set of fire estimates but our analyses showed that the impact of using GFED4 versus GFED2 on estimated Asia fluxes is very weak.

2.3 Atmospheric CO_2 observations

In this study, two sets of atmospheric CO_2 observation data were assimilated as follows: (1) surface CO_2 observations distributed by NOAA-ESRL (http://www.esrl.noaa.gov/gmd/ccgg/obspack/, data version 1.0.2) and by the WDCGG (World Data Centre for Greenhouse Gases, http://ds.data.jma.go.jp/gmd/wdcgg/) for the period 2006–2010 (the Asian surface site information is summarized in Fig. 1a and the global surface sites in Table S1 of the Supplement). Individual time series in this surface set were provided by many individual PIs (Principal Investigators) which we kindly acknowledge; (2) for the free tropospheric CO_2 observations, we use the aircraft measurements from the CONTRAIL project for the period 2006–2010 (see Fig. 1b).

A summary of Asian surface sites used in this study is shown in Table 1 and Fig. 1a for reference. There are fourteen surface sites with over 7957 observations located in Asia, including ten surface flask stations and four surface continuous sites. The surface CO_2 mole fraction data used in this study are all calibrated against the same CO_2 standard (WMO-X2007) (The World Meteorological Organization CO_2 mole fraction scale for 2007). For most of the continuous sampling sites at the surface, we derived an averaged afternoon CO_2 concentration (12:00–16:00, local time) for each day from the time series, while at mountain-top sites we constructed an average based on nighttime hours (00:00–04:00, local time) to reduce local influence and compare modeled with observed values only for well-mixed conditions.

We note that from the CONTRAIL program (Machida et al., 2008; Matsueda et al., 2008), stratospheric CO_2 data were not included into CTDAS because the stratospheric

Table 1. Summary of the 14 Asian surface CO_2 observation sites assimilated between 1 January 2006 and 31 December 2010. The frequency of continuous data is one per day (when available), while discrete surface data point is generally available once per week. MDM (model–data mismatch) is a value assigned to a given site that is meant to quantify our expected ability to simulate observations and used to calculate the innovation X^2 (Inn. X^2) statistics. N denotes the number of observations used in CTDAS. Flagged observations refer to a model-minus-observation difference that exceeds 3 times the model–data mismatch, these observations are therefore excluded from assimilation. The bias is the average from posterior residuals (assimilated values–measured values), while the modeled bias is the average from prior residuals (modeled values–measured values).

Site	Name	Lat, Lon, Elev.	Lab	N (flagged)	MDM	Inn. X^2	Bias(modeled)
Discrete samples in Asia:							
1 WLG	Mt. Waliguan, China	36.29° N, 100.90° E, 3810 m	CMA/ESRL	254(19)	1.5	0.83	−0.10(−0.14)
2 BKT	Bukit Kototabang, Indonesia	0.20° S, 100.312° E, 864 m	ESRL	172(0)	7.5	0.73	5.53(5.51)
3 WIS	Sede Boker, Israel	31.13° N, 34.88° E, 400 m	ESRL	239(1)	2.5	0.62	−0.10(−0.15)
4 KZD	Sary Taukum, Kazakhstan	44.45° N, 77.57° E, 412 m	ESRL	167(6)	2.5	1.16	−0.08(0.50)
5 KZM	Plateau Assy, Kazakhstan	43.25° N, 77.88° E, 2519 m	ESRL	155(2)	2.5	0.96	0.50(0.63)
6 TAP	Tae-ahn Peninsula, South Korea	36.73° N, 126.13° E, 20 m	ESRL	181(3)	7.5	0.60	1.82(2.13)
7 UUM	Ulaan Uul, Mongolia	44.45° N, 111.10° E, 914 m	ESRL	231(5)	2.5	1.17	0.10(0.28)
8 CRI	Cape Rama, India	15.08° N, 73.83° E, 60 m	CSIRO	33(1)	3	1.40	−1.97(−2.11)
9 LLN	Lulin, Taiwan	23.47° N, 120.87° E, 2862 m	ESRL	220(20)	7.5	0.99	2.62(2.65)
10 SDZ	Shangdianzi, China	40.39° N, 117.07° E, 287 m	CMA/ESRL	60(15)	3	1.18	0.15(0.18)
continuous samples in Asia:							
11 MNM	Minamitorishima, Japan	24.29° N, 153.98° E, 8 m	JMA	1624(0)	3	0.76	0.15(0.16)
12 RYO	Ryori, Japan	39.03° N, 141.82° E, 260 m	JMA	1663(48)	3	0.90	0.46(0.69)
13 YON	Yonagunijima, Japan	24.47° N, 123.02° E, 30 m	JMA	1684(3)	3	0.78	1.53(1.67)
14 GSN	Gosan, Republic of South Korea	33.15° N, 126.12° E, 72 m	NIER	1274(109)	3	1.99	−1.01(−0.82)

observations had a seasonal phase shifting and its smaller amplitude was difficult to compare to the tropospheric measurements (Sawa et al., 2008). A summary of the CONTRAIL aircraft measurements is presented in Table 2 and Fig. 1b. The CONTRAIL aircraft data are reported on the NIES (the National Institute for Environmental Studies) 09 CO_2 scale, which are lower than the WMO−X2007 CO_2 scale by 0.07 ppm at around 360 ppm and consistent in the range between 380 and 400 ppm (Machida et al., 2011). Thus the CONTRAIL CO_2 data sets are comparable to surface data. We follow the method from Niwa et al. (2012) to divide the data into four vertical bins (575–625, 465–525, 375–425, 225–275 hPa) from ascending and descending profiles and one vertical bin (225–275 hPa) from level cruising. We also divide CONTRAIL data into 42 horizontal bins/regions (Fig. 1b), which amounts to a total of 65 bins. Before daily averaging the CONTRAIL measurements for each 65 regional/vertical bins, we pre-process the aircraft data to obtain free troposphere CO_2 values by filtering out the stratospheric CO_2 data using a threshold of potential vorticity (PV) > 2 PVU (Potential Vorticity Unit, $1\,\mathrm{PVU} = 10^{-6}\,\mathrm{m^2\,s^{-1}\,K\,kg^{-1}}$), in which PV is calculated from TM5 (using ECMWF temperature, pressure and wind fields) (Sawa et al., 2008). A total number of 10 467 CO_2 aircraft observations over Asia have been used during the period from January 2006 to December 2010 in our inversion.

2.4 Sensitivity experiments and uncertainty estimation

Because the Gaussian uncertainties strongly depend on choices of prior errors in CTDAS, the formal covariance estimates for each week of optimization only reflect the random component of the inversion problem rather than a characterization of the true uncertainties of the estimated CO_2 flux. As an alternative, we performed a set of sensitivity experiments to obtain a more representative spread in the flux estimates and complement the formal Gaussian uncertainty estimates. We take different plausible alternative settings in CTDAS to design a more comprehensive sensitivity test, and use the minimum and maximum flux inferred in these experiments to present the range of the true flux. The following six inversions were performed to investigate the uncertainty span in this study:

Case 1: prior flux as in Sect. 2.2 + observations as in Sect. 2.3 + TM5 transport model runs at global 3° × 2° and a 1° × 1° nested grid over Asia. This is the base simulation (quoted as surface–CONTRAIL) which is used to analyze the 5 year carbon balance in this study.

Case 2: same as Case 1, but excluding CONTRAIL observations. We use these results (quoted as surface–only) to examine the impact of CONTRAIL data on Asian flux estimates by comparison with Case 1.

Case 3: like Case 1, but CTDAS runs with the updated fossil fuel emissions based on Wang et al. (2012) over China.

Table 2. Summary of the Asian CONTRAIL CO_2 observation data assimilated between 2006 and 2010. MDM (model–data mismatch) is a value assigned to a given site that is meant to quantify our expected ability to simulate observations and used to calculate the innovation X^2 (Inn. X^2) statistics. N denotes the number available in CTDAS. Flagged observations mean a model-minus-observation difference that exceeds 3 times the model–data mismatch, these data are therefore excluded from assimilation. The bias is the average of the posterior residuals (assimilated values–measured values), while the modeled bias is the average of prior residuals (modeled values–measured values).

Pressure Level	N(flagged)	MDM	Inn.X^2	Bias(modeled)
575–625 hPa	0	2.00	0.00	0.00
475–525 hPa	2907(5)	2.00	0.35	0.05(0.08)
375–425 hPa	3035(3)	2.00	0.34	−0.05(−0.07)
225–275 hPa	4525(4)	2.00	0.34	0.04(0.05)

Different from fossil fuel data in Case 1, the data of Wang et al. (2012) calculated carbon emissions from energy consumption, transportation, household energy consumption, commercial energy consumption, industrial processes and waste. And the seasonal variations between the two data sets are different. the fossil fuel emissions in Case 1 had the largest carbon emission in January and the smallest carbon source in July every year, while data of Wang et al. (2012) had the smallest fossil-fuel CO_2 emissions in February or March. This simulation is meant to partly address the impact of uncertainty in fossil fuel emissions over the region as suggested by Francey et al. (2013).

Case 4: like Case 1, but CTDAS runs based on 110 % of prior biosphere flux derived from CASA-GFED2;

Case 5: like Case 2, but the TM5 transport model is used at global $6° \times 4°$ without nested grids. This tests the impact of model resolution;

Case 6: like Case 2, but replacing the underlying land use map with MODIS data (Friedl et al., 2002) and keeping the number of ecoregions unchanged. The MODIS land use maps can be found in Fig. S1 in the Supplement.

The Cases 1 and 2 span the period 2006–2010 (the period 2004–2005 was discarded as spin-up), while the other sensitivity experiments were done from 2008 to 2010 only when the observational coverage was best. In general, these six sensitivity tests investigate most variations in the components of the assimilation framework. These variations are prior fluxes, observations available, the ecoregion map, the fossil fuel emissions, and transport. They also give alternative choices for the main components of the system. The sensitivity results are summarized in Table 3 and further discussed in the next section.

3 Results

We will from here on refer to carbon sinks with a negative sign, sources are positive, and will include the sign also when discussing anomalies (positive = less uptake or larger source, negative = more uptake or smaller source). We describe the results mainly over Asia (global flux estimates can be found in Table S2 in the Supplement), where we expected the CONTRAIL data to provide the additional constraints. Note that the results of Case 1 are analyzed as the best assimilation for the period of 2006–2010 in this study.

3.1 CO_2 concentration simulations

First we checked the accuracy of the model simulation using the surface CO_2 concentration observations and CONTRAIL aircraft CO_2 measurements. Figure 2a shows the comparison of modeled (both prior and posterior) CO_2 concentration with measurements at the discrete surface site of Mt. Waliguan (WLG, located at 36.29° N, 100.90° E). Note that the prior CO_2 concentrations here are not really based on a priori fluxes only, as they are a forecast started from the CO_2 mixing ratio field that contains all the already optimized fluxes $(1, ..., n-1)$ that occurred before the current cycle of the data assimilation system (n). So these prior mole fractions only contain five weeks of recent un-optimized fluxes and constitute our "first-guess" of atmospheric CO_2 for each site. For the WLG site, the comparison of the surface CO_2 time series shows that the modeled (both prior and posterior) CO_2 concentration is in general agreement with observed data during the period 2006–2010 (correlation coefficient $R = 0.87$), although the modeled result still could not adequately reproduce all the observed CO_2 seasonal variations. The posterior annual model–observation mismatch of this distribution is -0.10 ± 1.25 ppm, with 0.07 ± 1.50 ppm bias for the summer period (June–July–August) and 0.02 ± 0.80 ppm bias for the winter period (December–January–February). The model–observation mismatch is a little larger in Case 2 without CONTRAIL data (model–observation mismatch: -0.13 ± 1.26 ppm), suggesting that the surface fluxes derived with CONTRAIL agree with the surface CO_2 mixing ratios at WLG station. Over the full study period, the WLG modeled mole fractions exhibit good agreement with the observed CO_2 time series and the changes in inferred mixing ratios/flux are within the specified uncertainties in our inversion system, an important prerequisite for a good flux estimate.

We also checked the inversion performance in the free troposphere in addition to the surface CO_2. Figure 2b, c and d show the comparison between measured and modeled (both prior and posterior) mixing ratios in the free troposphere during the period from 2006–2010 in the region covering 32–40° N, 136–144° E for three vertical bins (475–525, 375–425, 225–275 hPa). The observed vertical CO_2 patterns were reasonably reproduced by our model, with high correlation

Table 3. Results of the sensitivity experiments conducted in this study (units of Pg C yr^{-1})*.

Inversion ID	Case 1	Case 2	Case 3	Case 4	Case 5	Case 6
Boreal Eurasia	−1.02	−0.96	−1.11	−1.25	−1.03	−0.92
Temperate Eurasia	−0.68	−0.33	−0.70	−0.63	−0.37	−0.36
Tropical Asia	0.15	0.19	0.12	0.08	0.17	0.20
Total Asia	−1.56	−1.09	−1.69	−1.80	−1.23	−1.07
NH land sink	−2.93	−2.64	−3.20	−3.20	−2.79	−2.70
Land	−2.43	−2.24	−3.07	−3.25	−2.65	−2.50
Ocean	−2.08	−2.16	−2.04	−2.05	−2.27	−2.18
Global	−4.50	−4.41	−5.12	−5.30	−4.92	−4.68

* The Case 1 (surface-CONTRAIL) and Case 2 (surface–only) were simulated for the period 2006–2010, while Case 3–6 was simulated for the period 2008–2010; detailed discussion on global flux estimates can be found in Table S2 in the Supplement.

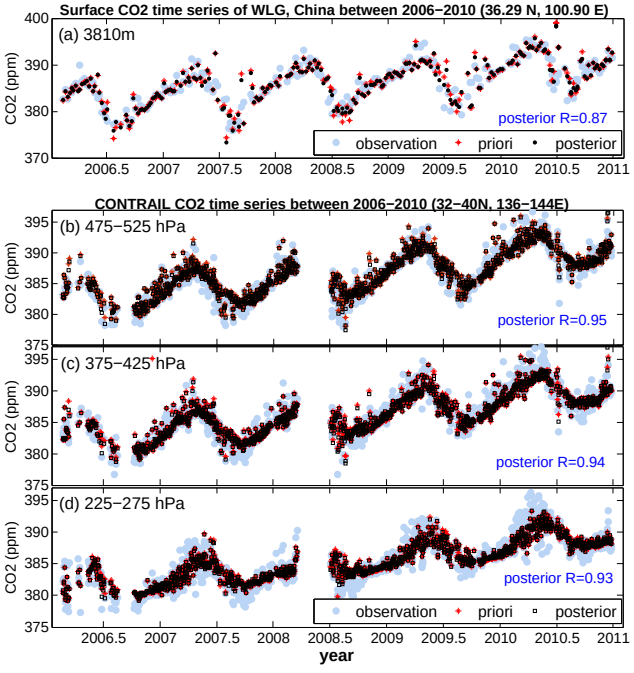

Figure 2. Comparison of modeled values with observed CO_2 concentrations from surface flask station **(a)** Mt. Waliguan (WLG), located in China; and from CONTRAIL data in the region covering 32–40° N, 136–144° N for the following three different vertical bins: **(b)** 475–525 hPa; **(c)** 375–425 hPa; **(d)** 225–275. Although four vertical bins (575–625, 475–525, 375–425, 225–275 hPa) of CONTRAIL measurements have been selected and added into the system, only three vertical bin observations have really been assimilated as sparse measurements associated with the 575–625 hPa in CONTRAIL data. Note that the prior CO_2 concentrations here are not really based on a priori fluxes only, as they are a forecast started from the CO_2 mixing ratio field that contains all the already optimized fluxes (1, ..., $n-1$) that occurred before the current cycle of the data assimilation system (n). So these prior mole fractions only contain five weeks (five weeks are the lag windows in our system) of recent un-optimized fluxes and constitute our "first guess" of atmospheric CO_2 for each site.

coefficient ($R = 0.95$, 0.94 and 0.93 for 475–525, 375–425, 225–275 hPa, respectively) between CONTRAIL and (posterior) modeled CO_2. The observed low vertical gradients for flight sections in three vertical bins (475–525, 375–425, 225–275 hPa) at northern mid-latitudes (32–40° E) were well captured by the model (both prior and posterior), indicating the transport model can reasonably produce the vertical structure of observations.

We found that the observed CO_2 concentration profiles were modeled better after assimilation than before (modeled − observed $= 0.05 \pm 1.25$ ppm for a priori and -0.01 ± 1.18 ppm for posterior), although our inverted (posterior) mole fractions still could not adequately reproduce the high values in winter (December–January–February) and the low values in summer (June–July–August). This mismatch of CO_2 seasonal amplitude suggests that our inverted (posterior) CO_2 surface fluxes do not catch the peak of terrestrial carbon exchange well. Previous studies have also found this seasonal mismatch, which may correlate with atmospheric transport, and has already been identified as a shortcoming in most inversions (Peylin et al., 2013; Saeki et al., 2013; Stephens et al., 2007; Yang et al., 2007). In addition, we found that the optimized CO_2 mole fractions seem better captured at low altitude with smaller standard deviations of the model–observation mismatch (±1.12, ±1.18 and ±1.26 ppm for 475–525, 375–425, 225–275 hPa) and higher correlation coefficient at 475–525 hPa. This suggests that the near surface layers are comparatively well constrained in CTDAS. Overall, the agreement between the model and measurements is fairly good and consistent with previously known behavior in the CarbonTracker systems, derived mostly from North American and European continuous sites. Note that all model–observation mismatch of Asian surface sites and CONTRAIL data have been included in Tables 1 and 2 (see column of "Bias (modeled)").

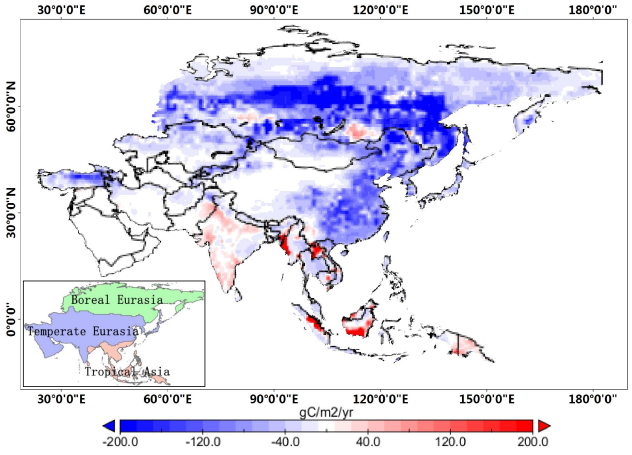

Figure 3. Mean terrestrial biosphere carbon flux estimated from our system over Asia during the period from 2006–2010 at a 1×1 grid resolution. Blue colors (negative) denote net carbon uptake while red colors (positive) denote carbon release to the atmosphere. Note that the estimated flux map includes net terrestrial fluxes and biomass-burning sources but excludes fossil fuel emissions.

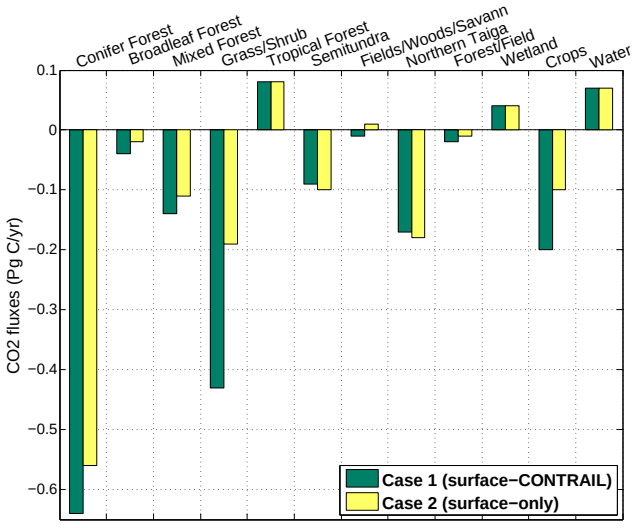

Figure 4. Fluxes per ecoregion in Asia averaged over the period 2006–2010 in Cases 1 and 2 (in $\mathrm{Pg\,C\,yr^{-1}}$).

3.2 Inverted Asian terrestrial CO_2 flux

3.2.1 Five-year mean

During the period from 2006–2010, we found a mean net terrestrial land carbon uptake (a posteriori) in Asia of $-1.56\,\mathrm{Pg\,C\,yr^{-1}}$, consisting of $-2.02\,\mathrm{Pg\,C\,yr^{-1}}$ uptake by the terrestrial biosphere and $+0.47\,\mathrm{Pg\,C\,yr^{-1}}$ release by biomass-burning (fire) emissions (Table 6). This terrestrial uptake compensates 38 % of the estimated $+4.15\,\mathrm{Pg\,C\,yr^{-1}}$ CO_2 emissions from fossil fuel burning and cement manufacturing in Asia. An uncertainty analysis for the Asian terrestrial CO_2 uptake derived from a set of sensitivity experiments has been conducted and put the estimated sink in a range from -1.07 to $-1.80\,\mathrm{Pg\,C\,yr^{-1}}$ (Table 3), while the 1-sigma of the formal Gaussian uncertainty estimate is $\pm 1.18\,\mathrm{Pg\,C\,yr^{-1}}$ (Table 6). The estimated Asian net terrestrial CO_2 sink is further partitioned into a $-1.02\,\mathrm{Pg\,C\,yr^{-1}}$ carbon sink in boreal Eurasia and a $-0.68\,\mathrm{Pg\,C\,yr^{-1}}$ carbon sink in temperate Eurasia, with a $+0.15\,\mathrm{Pg\,C\,yr^{-1}}$ CO_2 source in tropical Asia.

The annual mean spatial distribution of net terrestrial carbon uptake over Asia is shown in Fig. 3. Note that the estimated fluxes include terrestrial fluxes and biomass-burning sources but exclude fossil fuel emissions. Most Asian regions were natural carbon sinks over the studied period, with the strongest carbon uptake in the middle and high latitudes of the Northern Hemispheric part of Asia, while the low-latitude region releases CO_2 to the atmosphere. This flux distribution pattern is quite consistent with previous findings that northern temperate and high latitude ecosystems were large sinks (Hayes et al., 2011) and tropical land regions were carbon sources (Gurney et al., 2003).

The aggregated terrestrial CO_2 fluxes 19 different ecosystems (Fig. 1a) averaged over the period 2006–2010 are shown in Tables 4 and 5 and Fig. 4 (see Case 1). The majority of the carbon sink was found in the regions dominated by forests, crops and grass/shrubs. The largest uptake is by the forests with a mean sink of $-0.77\,\mathrm{Pg\,C\,yr^{-1}}$, 83 % of which ($-0.64\,\mathrm{Pg\,C\,yr^{-1}}$) was taken up by conifer forests and 18 % of which ($-0.14\,\mathrm{Pg\,C\,yr^{-1}}$) by mixed forest, whereas the tropical forests released CO_2 ($+0.08\,\mathrm{Pg\,C\,yr^{-1}}$). The estimated flux by CTDAS in Asian cropland ecosystems was $-0.20\,\mathrm{Pg\,C\,yr^{-1}}$, with the largest crop carbon sink located in temperate Eurasia ($-0.17\,\mathrm{Pg\,C\,yr^{-1}}$). The grass/shrub lands in Asia absorbed $-0.44\,\mathrm{Pg\,C\,yr^{-1}}$, with most of these grass/shrub sinks located in temperate Eurasia ($-0.36\,\mathrm{Pg\,C\,yr^{-1}}$). Other land-cover types (e.g., wetland, semi tundra and so on) sequestered about $-0.15\,\mathrm{Pg\,C\,yr^{-1}}$ (10 % of total) over Asian regions. This suggests that according to our model, many ecosystems contributed to Asian CO_2 sinks, highlighting the complexity of the total northern hemispheric sinks.

Also, we note that the detailed CO_2 flux partitioning in our assimilation system highly relies on the prior model description of the ecosystem-by-ecosystem flux patterns. To evaluate the Gaussian errors of the CO_2 flux estimate for a related ecosystem type, we calculated the posterior/prior Gaussian errors (1-sigma) as well as the error reduction for individual ecosystem types during the period 2006–2010 (Table 5). As shown in Table 5, the uncertainty reduction rates are 24.30 %, 23.81 % and 23.81 % for forestlands, Grass/Shrub ecosystems and croplands, respectively. This error reduction suggests that the inferred carbon sink partitioning for individual

ecosystem types are to some extent constrained by the assimilation system. However, a large uncertainty still exists in the posterior carbon sink for most ecosystem types.We can make the assumption that the correlation between two inverted ecosystem-related fluxes indicates how well the ecosystem-related estimation of carbon fluxes is being constrained by the observations (lower correlation, stronger constrained; while higher correlation, weaker constrained), to further explore the optimized carbon fluxes during the period 2006–2010 (data shown in Table 4). As shown in Fig. 5, the absolute values of posterior correlation coefficients are less than 0.5 (most in the range of -0.3 to 0.5), while they started uncorrelated (0.0). This confirms that ecoregion fluxes have not been fully independently retrieved.

3.2.2 Seasonal variability

Figure 6 shows the prior and posterior seasonal cycles of CO_2 fluxes for the Asia region and its three sub-regions as well as their Gaussian uncertainties. The seasonal amplitude in boreal Eurasia as shown in Fig. 6b proves to be the major contributor to the seasonal signal in Asia (Fig. 6a). The large uptake of boreal Eurasia occurs in summer and the large differences between the prior and the posterior fluxes are also found in the summer growing season, indicating the surface observation network and CONTRAIL data largely affect the estimated fluxes. Our monthly variability is very close to changes in boreal Eurasia presented by Gurney et al. (2004). In Fig. 6c, the seasonal pattern for the temperate Eurasia region shows a comparable pattern to boreal Eurasia but with a smaller seasonal magnitude. And the adjustments of the prior flux in spring and summer are also smaller. The largest CO_2 uptake in temperate Eurasia subregion, however, is shifted from July to August compared to boreal Eurasia, suggesting that a phase shift in the growing season occurred here with the highest CO_2 sink occurring later in the year. This seasonal cycle is slightly different from that reported by Gurney et al. (2004), but shows a nice agreement with the seasonal dynamics of Niwa et al. (2012) in the Southern temperate Asia region, and of Patra et al. (2011) in the Northwest Asia region. In tropical Asia (Fig. 6d), the seasonal variation is very different from other Asian subregions characterized by a weak CO_2 uptake peak in August–October and much smaller carbon release in May–July. Overall, the posterior uncertainty reduction for the period 2006–2010 was about 25 % in Asia, with the largest uncertainty remaining in the summer, suggesting that our model may not fully capture the biosphere sink signal in the growing season.

3.2.3 Interannual variability (IAV)

Figure 7 shows the estimated annual cumulative net ecosystem exchange in Asia during the period from 2006–2010 as well as its anomaly with weekly intervals. Here, the biomass-burning and fossil fuel emissions are excluded, and only the sum of fluxes from respiration and photosynthesis are shown, because biomass-burning emissions have large interannual variability, especially for tropical Asia.

The coefficient of IAV (IAV = standard deviation/mean) in Asian land carbon flux is 0.12, with a peak-to-peak amplitude of $0.57\,\mathrm{Pg\,C\,yr^{-1}}$ (amplitude = smallest – largest CO_2 sink), ranging from the smallest carbon uptake of $-1.71\,\mathrm{Pg\,C\,yr^{-1}}$ in 2010 and the largest CO_2 sink of $-2.28\,\mathrm{Pg\,C\,yr^{-1}}$ in 2009. As has been noted in many other studies (Gurney et al., 2004, 2008; Mohammat et al., 2012; Patra et al., 2011; Peters et al., 2007, 2010; Yu et al., 2013), the IAV of the carbon flux strongly correlates with climate factors, such as air temperature, precipitation and moisture.

The year 2010 stands out as a particularly low uptake year in Asia, with a reduction of terrestrial uptake of $0.31\,\mathrm{Pg\,C\,yr^{-1}}$ compared to the five-year mean. This reduction mainly appeared in temperate Eurasia and ropical Asia, leading to $+0.25\,\mathrm{Pg\,C\,yr^{-1}}$ (35 % sink reduction) and $+0.04\,\mathrm{Pg\,C\,yr^{-1}}$ flux anomalies (24 % sink reduction) in their corresponding regions. In 2010, Asia experienced a set of anomalous climate events. For example, temperate Eurasia experienced a severe spring/autumn drought, and a heavy summer flood and a heat wave occurred in 2010 (National Climate Center, 2011). From Fig. 7b, we can see that 2010 did not show large anomalies until after the spring growing season. As anomalous climate appeared, the summer flood and autumn drought were identified as dominant climatic factors controlling vegetation growth and exhibiting a significant correlation with the land carbon sink, particularly in the croplands, grasslands and forests of temperate Eurasia. In the end, 2010 only showed $-1.71\,\mathrm{Pg\,C\,yr^{-1}}$ biospheric CO_2 uptakes (excluding fires) by the end of the year.

In contrast to 2010, the year 2009 had the strongest carbon sink for the study period, with much stronger uptake in temperate Eurasia ($-0.20\,\mathrm{Pg\,C\,yr^{-1}}$ anomaly, 28 % increase in CO_2 uptake) as well as in boreal Eurasia ($-0.05\,\mathrm{Pg\,C\,yr^{-1}}$ anomaly, 4 % uptake increase compared to the five-year mean). It can be seen that 2009 started with a lower-than-average release of carbon in the first 4 months (17 weeks) of the year amounting to $+0.28\,\mathrm{Pg\,C\,yr^{-1}}$ compared to the five-year average of $+0.45\,\mathrm{Pg\,C\,yr^{-1}}$. This variation of the Asian terrestrial carbon sink in the spring vegetation growing season may partly relate to a higher spring temperature in 2009 which induced an earlier onset of the growing season and led to a high vegetation productivity by extending the growing season (Mohammat et al., 2012; Richardson et al., 2009; Walther et al., 2002; Wang et al., 2011; Yu et al., 2013). From Fig. 7b, 2009 shows a very high carbon uptake in the summer growing season (June–August, weeks 22 to 32) concurrent with favorable temperature and abundant precipitation conditions. After this summer, the vegetation productivity returned back to normal and the total cumulative carbon sink added up to $-2.28\,\mathrm{Pg\,C\,yr^{-1}}$ at the end of the year with $-0.26\,\mathrm{Pg\,C\,yr^{-1}}$ extra uptake compared to the five-year mean.

Table 4. The ecosystem-type associated posterior terrestrial biosphere fluxes for 2006–2010 (units of $Pg\,C\,yr^{-1}$).

	type	Asia	Boreal Eurasia	Temperate Eurasia	Tropical Asia
Forest	Total	−0.77	−0.71	−0.11	0.04
	Conifer Forest	−0.64	−0.63	−0.02	0.00
	Broadleaf Forest	−0.04	−0.01	−0.01	−0.01
	Mixed Forest	−0.14	−0.05	−0.07	−0.03
	Fields/Woods/Savanna	−0.01	−0.01	0.00	0.00
	Forest/Field	−0.02	−0.01	−0.01	0.00
	Tropical Forest	+0.08	0.00	0.00	+0.08
Grass/Shrub	Total	−0.44	−0.06	−0.36	−0.02
	Grass/Shrub	−0.43	−0.06	−0.36	−0.02
	Scrub/Woods	0.00	0.00	0.00	0.00
	Shrub/Tree/Suc.	0.00	0.00	0.00	0.00
Crop	Crops	−0.20	−0.02	−0.17	−0.01
Others	Total	−0.15	−0.23	−0.04	0.13
	Semi-tundra	−0.09	−0.05	−0.04	0.00
	Northern Taiga	−0.17	−0.17	0.00	0.00
	Wooded tundra	0.00	0.00	0.00	0.00
	Mangrove	0.00	0.00	0.00	0.00
	Non-optimized	0.00	0.00	0.00	0.00
	Water	+0.07	0.00	0.00	+0.07
	Wetland	+0.04	−0.01	0.00	+0.06
	Deserts	0.00	0.00	0.00	0.00

Table 5. The posterior/prior Gaussian errors (1-sigma) as well as the error reduction rate for the ecosystem types for 2006–2010.

	type	Posterior(Prior) Gaussian errors ($Pg\,C\,yr^{-1}$)				Gaussian error reduction rate (%)*			
		Asia	Boreal Eurasia	Temperate Eurasia	Tropical Asia	Asia	Boreal Eurasia	Temperate Eurasia	Tropical Asia
Forest	Total	0.81(1.07)	0.74(0.98)	0.22(0.28)	0.26(0.31)	24.30 %	24.49 %	21.43 %	16.13 %
	Conifer Forest	0.71(0.94)	0.71(0.94)	0.05(0.06)	0(0)	25.43 %	25.53 %	16.33 %	–
	Broadleaf Forest	0.12(0.14)	0.05(0.06)	0.1(0.12)	0.04(0.04)	14.29 %	16.67 %	16.67 %	0.00 %
	Mixed Forest	0.27(0.33)	0.21(0.25)	0.16(0.2)	0.04(0.05)	18.18 %	16.00 %	20.00 %	20.00 %
	Fields/Woods/Savanna	0.11(0.14)	0.05(0.06)	0.10(0.13)	0.01(0.02)	12.43 %	11.67 %	12.08 %	11.00 %
	Forest/Field	0.10(0.12)	0.08(0.09)	0.04(0.06)	0.05(0.06)	16.67 %	11.11 %	33.33 %	16.67 %
	Tropical Forest	0.25(0.30)	0(0)	0.05(0.06)	0.25(0.3)	16.67 %	–	16.67 %	16.67 %
Grass/Shrub	Total	0.48(0.63)	0.17(0.2)	0.45(0.59)	0.05(0.06)	23.81 %	21.85 %	14.73 %	22.67 %
	Grass/Shrub	0.48(0.63)	0.17(0.2)	0.45(0.59)	0.05(0.06)	23.81 %	21.85 %	14.73 %	22.67 %
	Scrub/Woods	0(0)	0(0)	0(0)	0(0)	–	–	–	–
	Shrub/Tree/Suc.	0(0)	0(0)	0(0)	0(0)	–	–	–	–
crop	Crops	0.48(0.63)	0.09(0.11)	0.46(0.61)	0.1(0.12)	23.81 %	18.18 %	24.59 %	16.67 %
Others	Total	0.52(0.64)	0.48(0.6)	0.19(0.23)	0.02(0.02)	18.75 %	20.00 %	17.39 %	0.00 %
	Semi-tundra	0.35(0.43)	0.3(0.36)	0.19(0.23)	0(0)	18.60 %	16.67 %	17.39 %	–
	Northern Taiga	0.36(0.45)	0.36(0.45)	0(0)	0(0)	20.00 %	20.00 %	–	–
	Wooded tundra	0(0)	0(0)	0(0)	0(0)	–	–	–	–
	Mangrove	0(0)	0(0)	0(0)	0(0)	–	–	–	–
	Non-optimized	0(0)	0(0)	0(0)	0(0)	–	–	–	–
	Water	0.00(0.00)	0(0)	0(0)	0.00(0.00)	8.70 %	–	–	8.70 %
	Wetland	0.1(0.12)	0.10(0.12)	0.0(0.0)	0.02(0.02)	16.67 %	11.67 %	11.40 %	18.00 %
	Deserts	0(0)	0(0)	0(0)	0(0)	–	–	–	–

* Gaussian error reduction rate is calculated as follows: $(\sigma_{prior} - \sigma_{posterior})/\sigma_{prior} \times 100$.

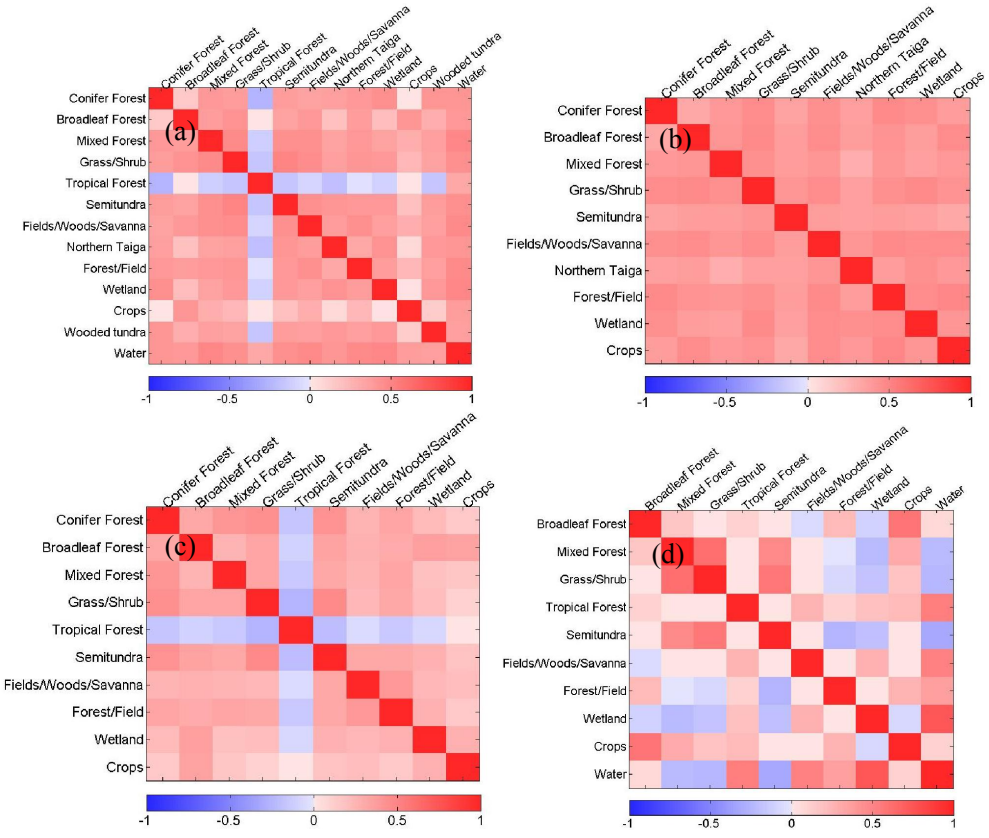

Figure 5. The matrixes of the ecosystem-by-ecosystem paired correlations for the optimized carbon fluxes during the period 2006–2010 are **(a)** Asia; **(b)** boreal Eurasia; **(c)** temperate Eurasia; **(d)** tropical Asia.

3.2.4 Uncertainty estimation

Table 3 presents the estimated annual mean NEE across the alternative sensitivity experiments. The time spans are different among six tests. Case 1 (surface-CONTRAIL) and Case 2 (surface-only) run for the period 2006–2010 (the period 2004–2005 servers as a spin-up period), while Cases 3 to 6 run for the period 2008–2010. To compare other alternative sensitivity estimates for the same period from 2008–2010, we calculated this three-year average of annual Asia CO_2 fluxes (the period 2008–2010) from all the six tests to be -1.61, -1.15, -1.69, -1.80, -1.23 and -1.07 PgC yr^{-1}, respectively. The Asian CO_2 uptake thus ranges from -1.07 to -1.80 Pg C yr^{-1} across our sensitivity experiments, which complements the Gaussian error. Despite the small numbers of years included, this range suggests that the Asian terrestrial was a sizable sink, while a carbon source implied in previous studies by the 1-sigma Gaussian error of ± 1.18 Pg C yr^{-1} on the estimated mean, is very unlikely. The largest sensitivity in inferred flux is to the change of prior terrestrial biosphere fluxes (Case 4, difference = Case 4 – Case 1). The inversions with different model resolutions (Case 5, difference = Case 5 – Case 2) and with different Chinese fossil fuel emissions (Case 3, difference = Case 4 – Case 1) also show large variations in the inverted CO_2 fluxes, while the sensitivity to the change of land cover types (Case 6, difference = Case 6 – Case 2) is generally modest. This highlights the current uncertainties in the Asian sink and the best method to estimate it from inverse modeling.

3.2.5 Impacts of the CONTRAIL data on inverted Asian CO_2 flux

We examined the impacts of the CONTRAIL data on Asian flux estimation by comparing results from Case 1 (surface-CONTRAIL) and Case 2 (surface-only) (Table 6 and Fig. 8a). Note that the uncertainties shown in the Table 6 and Fig. 8b are now the Gaussian uncertainties as we did not repeat all sensitivity experiments. As shown in Table 6, inclusion of the CONTRAIL data induces an averaged extra CO_2 sink of about -0.47 Pg C yr^{-1} to Case 1 ($0.47 = 1.56–1.09$), with most addition to the grass/shrub ecosystem (Fig. 4). The spatial pattern of Asian fluxes also changed considerably (see Fig. 8a). For instance, a decrease in CO_2 uptake was found in the northern area of boreal Eurasia together with an increase in the south of boreal Eurasia, leading to almost identical total carbon sink strength in boreal Asia between with and without CONTRAIL data. Whereas the estimated flux

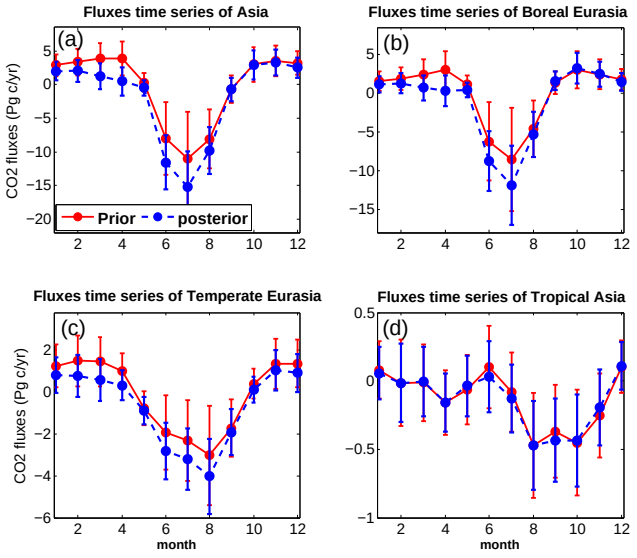

Figure 6. A priori and posteriori averaged fluxes (with uncertainties) over Asian regions during the period 2006–2010 are listed as follows: **(a)** Asia; **(b)** boreal Eurasia; **(c)** temperate Eurasia; **(d)** tropical Asia. This flux is biosphere carbon sink after removal of fossil and biomass-burning fluxes.

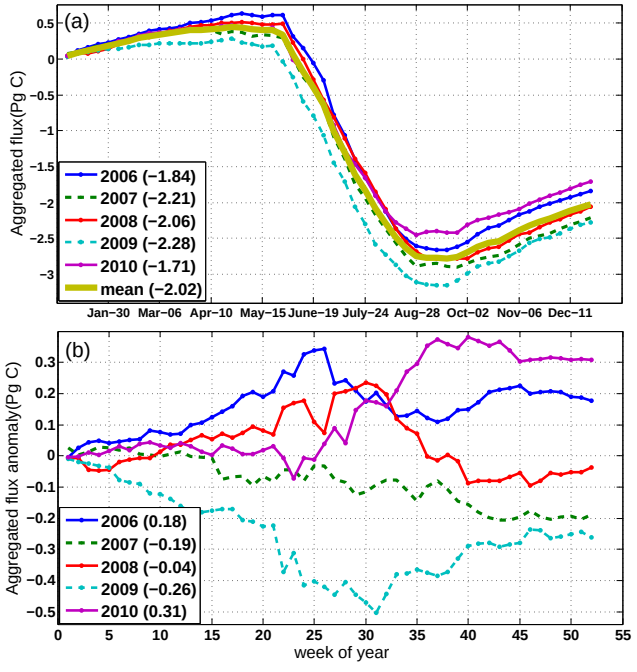

Figure 7. (a) Cumulative net Asian ecosystem exchange (NEE) vs. time estimated in our system for each of the individual years and for the 2006–2010 mean. This figure reveals the largest uptake in 2009 and the smallest uptake in 2010. **(b)** Cumulative anomaly of Asian CO_2 exchange through the years 2006 to 2010. The inferred Asian carbon fluxes shown here include only respiration and photosynthesis, because the biomass-burning emissions have a large interannual variability.

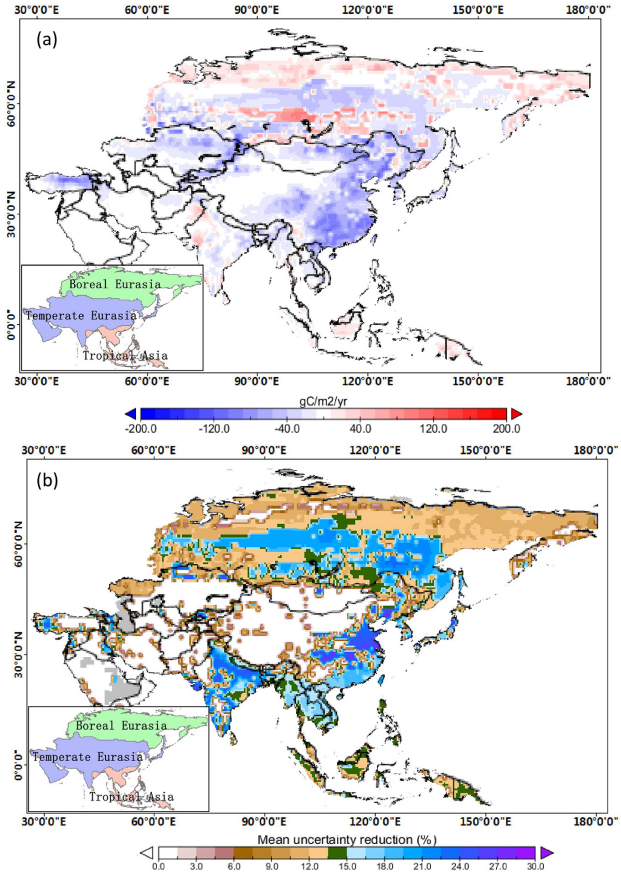

Figure 8. (a) The inverted flux difference between surface CO_2 observation data only surface (surface-only) and both the surface CO_2 observation data and CONTRAIL data (surface-CONTRAIL); and **(b)** the Gaussian error reduction rate between surface-only and surface-CONTRAIL during the period 2006–2010. The flux difference is derived from (surface-CONTRAIL – surface-only), while the Gaussian error reduction rate is calculated as $(\sigma_{\text{surface-only}} - \sigma_{\text{surface-CONTRAIL}})/\sigma_{\text{surface-only}} \times 100$.

distribution in tropical Asia showed a small spatial change and a large increase in regional sink size with CONTRAIL observations included.

Table 6 and Fig. 8b shows the reduction of the Gaussian error between Case 1 and Case 2. The error reduction rate (ER) is calculated as the following percentage:

$$\mathrm{ER} = \frac{(\sigma_{\text{surface-only}} - \sigma_{\text{surface-CONTRAIL}})}{\sigma_{\text{surface-only}} \times 100}, \quad (2)$$

where $\sigma_{\text{surface-only}}$ and $\sigma_{\text{surface-CONTRAIL}}$ are Gaussian errors in Case 2 (surface-only) and Case 1 (surface-CONTRAIL), respectively. By including the additional CONTRAIL data into the inversion system, the uncertainty of the posterior flux over Asia is significantly reduced (> 10 %), especially for the southeast of boreal Eurasia, southeast of temperate Eurasia and tropical areas (up to 20–30 %). The more pronounced reduction was found in boreal Eurasia and tropical

Table 6. The prior/posterior land fluxes, biomass-burning (fire) emissions, fossil fuel emissions and net land flux as well as the Gaussian error/their error reduction rates in surface-only and surface-CONTRAIL inversion experiments during the period 2006–2010 (in $\mathrm{Pg\,C\,yr^{-1}}$).

Region	Prior Land Flux	Fire Emission	Fossil-fuel Emission	Post. Land Flux		Post. Net Land Flux *		Gaussian error
				surface-only	surface-CONTRAIL	surface-only	surface-CONTRAIL	Error reduction (%)
Boreal Eurasia	-0.10 ± 1.16	0.13	0.21	-1.09 ± 1.05	-1.15 ± 0.91	-0.96 ± 1.05	-1.02 ± 0.91	14
Temperate Eurasia	-0.15 ± 0.93	0.03	3.31	-0.36 ± 0.75	-0.70 ± 0.70	-0.33 ± 0.75	-0.68 ± 0.70	6
Tropical Asia	-0.10 ± 0.35	0.32	0.63	-0.13 ± 0.33	-0.17 ± 0.28	0.20 ± 0.33	0.15 ± 0.28	15
Total Asia	-0.35 ± 1.53	0.47	4.15	-1.56 ± 1.34	-2.02 ± 1.18	-1.09 ± 1.34	-1.56 ± 1.18	11

* Posterior Net Land Flux including posterior land flux and fire emissions, but excluding fossil emissions.

Asia (reducing by 14 % and 15 %, respectively). This suggests that current surface CO_2 observations data alone do not sufficiently constrain these regional flux estimations (there are no observation sites in boreal Eurasia and only one in tropical Asia), and the additional CONTRAIL CO_2 observations impose an extra constraint that can help reduce uncertainty on inferred Asia CO_2 fluxes, especially for these two surface observation sparse regions.

4 Discussions and conclusions

4.1 Impact of CONTRAIL

Our modeling experiments reveal that the extra aircraft observations shift the inverted CO_2 flux estimates by imposing further constraints. This confirms the earlier findings by Saeki et al. (2003) and Maksyutov et al. (2013) that the inverted fluxes were sensitive to observation data used. For tropical Asia, inclusion of the CONTRAIL data notably reduced the uncertainties (about 15 % reduction). Compared with an inversion study with the CONTRAIL data for the tropical Asia region (Niwa et al., 2012) , the error reduction rate in land flux estimation in this study for the same region is smaller than that of Niwa et al. (34 %). This difference in uncertainty reduction likely results from the differences in inversion system design between these two studies, of which vertical mixing represented in transport model, and covariance assigned to prior fluxes are typically most important. We furthermore note that the set of observations used in these studies was not identical, we for instance included one tropical surface site (BKT, see Table 1 and Fig. 1a) to constrain the inferred flux estimation but Niwa, et al. (2012) did not.

Our results share other features with the Niwa et al. (2012) study, for instance the largest impact on the least data constrained regions. As reported by Niwa et al. (2012), the inclusion of CONTRAIL measurements not only constrains the nearby fluxes, but also reduces inferred flux errors in the regions far from the CONTRAIL measurement locations. For instance, in boreal Eurasia, where no surface site exists and which is far from the CONTRAIL data locations (after preprocessing of horizontal/vertical bins and filter operation of stratospheric, there is no CONTRAIL observation available over this region), uncertainty reductions are large (14 % reduction in uncertainty). Similar results were also presented by Niwa et al. (2012), with an 18 % error reduction in boreal Eurasia. These two studies consistently suggest that including the CONTRAIL measurements in inversion modeling systems will help to increase the NEE estimation accuracy over boreal Eurasia.

The CONTRAIL constraint on temperate Eurasia is generally modest, only having a 6 % error reduction. This may because temperate Eurasia has more surface observation sites than other regions in Asia. However, it is interesting that the difference in inverted NEE in this region between surface-only and surface-CONTRAIL is large ($-0.35\,\mathrm{Pg\,C\,yr^{-1}}$), but inconsistent with Niwa et al. (2012). One cause of this is likely the sensitivity of these inverse systems to vertical transport (Stephens et al., 2007), as also suggested by Niwa et al. (2012). The uneven distribution of observations at the surface and free troposphere may also aggravate this discrepancy.

4.2 Comparison of the estimated Asian CO_2 flux with other studies

Our estimated Asian terrestrial carbon sink is about $-1.56\,\mathrm{Pg\,C\,yr^{-1}}$ for the period 2006–2010. Most parts of Asian were estimated to be CO_2 sinks, with the largest carbon sink ($-1.02\,\mathrm{Pg\,C\,yr^{-1}}$) in boreal Eurasia, a second large CO_2 sink ($-0.68\,\mathrm{Pg\,C\,yr^{-1}}$) in temperate Eurasia, and a small source ($+0.15\,\mathrm{Pg\,C\,yr^{-1}}$) in tropical Asia. This spatial distribution of estimated terrestrial CO_2 fluxes is overall comparable to the results for the period of 2000–2009 by Saeki et al. (2013), derived from an inversion approach focusing on Siberia with additional Siberian aircraft and tower CO_2 measurements, especially in the high latitude areas.

Comparisons of our inverted CO_2 flux with previous studies are summarized in Table 7. In boreal Eurasia, our inferred land flux ($-1.02\,\mathrm{Pg\,C\,yr^{-1}}$) is higher than Gurney et al. (2003) ($-0.59\,\mathrm{Pg\,C\,yr^{-1}}$ during the period 1992–1996), but close to Maki et al. (2010) ($-1.46\,\mathrm{Pg\,C\,yr^{-1}}$ during the period 2001–2007), CTE2013 ($-0.93\,\mathrm{Pg\,C\,yr^{-1}}$) and CT2011_oi ($-1.00\,\mathrm{Pg\,C\,yr^{-1}}$, downloaded from http://carbontracker.noaa.gov). In Temperate Eurasia, our inverted flux is $-0.68\,\mathrm{Pg\,C\,yr^{-1}}$, which is well consistent with Gurney et al. (2003) ($-0.60\,\mathrm{Pg\,C\,yr^{-1}}$), but higher than CTE2013 ($-0.33\,\mathrm{Pg\,C\,yr^{-1}}$) and CT2011_oi

Table 7. Comparison of the inverted Asia terrestrial ecosystem carbon fluxes (in $Pg\,C\,yr^{-1}$) from this study with previous studies.

Reference	Period	Boreal Eurasia	Temperate Eurasia	Tropical Asia	Asia	Remarks
This study	2006–2010	-1.02 ± 0.91	-0.68 ± 0.70	$+0.15 \pm 0.28$	-1.56 ± 1.18	surface-CONTRAIL
(Gurney et al., 2003)	1992–1996	-0.59 ± 0.52	-0.60 ± 0.67	$+0.67 \pm 0.70$	-0.52 ± 0.65	–
(Maki et al., 2010)	2001–2007	-1.46 ± 0.41	0.96 ± 0.59	-0.15 ± 0.44	-0.65 ± 0.49	CNTL experiments
CTE2013[a]	2006–2010	-0.93 ± 1.15	-0.33 ± 0.56	$+0.22 \pm 0.20$	-1.05 ± 1.29	Focused on North America and Europe
CT2011_oi[b]	2006–2010	-1.00	-0.41	$+0.14$	-1.27	Focused on North America
(Niwa et al., 2012)[c]	2006–2008	-0.34 ± 0.23	-0.05 ± 0.27	$+0.45 \pm 0.19$	$+0.06 \pm 0.40$	GVCT
		-0.25 ± 0.28	-0.32 ± 0.32	$+0.03 \pm 0.29$	-0.54 ± 0.51	GV

[a] CTE2013: Carbon Tracker Europe in Peylin et al. (2013) for the period 2006–2010. [b] CT2011_oi: download from http://carbontracker.noaa.gov; without providing uncertainties; Note that that the CTE2013 and CT2011_oi estimates are not independent, and share the TM5 transport model and ObsPack observations sets, but differences in zoomed transport, state vector configuration and prior biosphere models used. [c] GVCT: jointly using GLOBALVIEW and CONTRAIL CO_2 observation data to perform inversion; GV: only GLOBALVIEW data used to conduct inversion; Note that the numbers of boreal Eurasia and temperate Eurasia and were obtained by personal communication.

Table 8. Comparison of IAVs of the terrestrial ecosystem carbon fluxes in Asia during the period 2006–2010 from this study with previous studies. Fluxes (in $Pg\,C\,yr^{-1}$) include biomass-burning emissions but exclude fossil fuel emissions.

year	Boreal Eurasia		Temperate Eurasia		Tropical Asia	
	This study	CTE2013	This study	CTE2013	This study	CTE2013
2006	−0.93	−0.93	−0.6	−0.4	0.37	0.41
2007	−1.17	−0.88	−0.8	−0.44	0.14	0.18
2008	−0.96	−1.07	−0.66	−0.33	−0.09	0.00
2009	−1.04	−0.78	−0.88	−0.34	0.12	0.25
2010	−1.01	−1.02	−0.49	−0.12	0.19	0.27

($-0.41\,Pg\,C\,yr^{-1}$) even though we used a similar inversion framework. One reason of this discrepancy is likely that different zoomed regions were configured in the inversion system. Another main factor is likely the inclusion of CONTRAIL largely impacts on our Temperate Eurasia's carbon estimates. In tropical Asia, our estimate is $+0.15\,Pg\,C\,yr^{-1}$, which is in the range of Niwa et al. (2012) ($+0.45\,Pg\,C\,yr^{-1}$, GVCT) and Patra et al. (2013) ($-0.104\,Pg\,C\,yr^{-1}$), both including aircraft CO_2 measurements in their inversion modeling, and very close to the CTE2013 ($+0.22\,Pg\,C\,yr^{-1}$) and CT2011_oi ($+0.14\,Pg\,C\,yr^{-1}$). The estimated total Asian terrestrial carbon sink is $-1.56\,Pg\,C\,yr^{-1}$, which is close to the CTE2013 ($-1.05\,Pg\,C\,yr^{-1}$) and CT2011_oi ($-1.27\,Pg\,C\,yr^{-1}$). The IAVs comparison between the results from this study and from CTE2013 is also presented in Table 8 (different from IAV in Sect. 3.2.2, these results include biomass-burning emissions). The IAVs are different between inferred terrestrial CO_2 flux of this study and CTE2013. In boreal Eurasia, there was a moderate Asian CO_2 sink in 2007 for CTE2013, while the results from this study show the highest carbon uptake for this year; in CTE2013, the strongest terrestrial CO_2 sink occurs in 2008, while from our estimates the sink in 2008 was weaker than that in 2007. For temperate Eurasia, the highest land sink occurs in 2007 for CTE2013, while in this study, the highest occurs in 2009. In tropical Asia, there is very similar IAVs between CTE2013 and this study, but the size of the carbon sink is inconsistent. Differences likely stems from the additions of Asian sites and CONTRAIL data in this study. Compared to previous findings, our updated estimation with these additional data seems to support a larger Asian carbon sink over the past decade.

The spatial patterns of NEE in Asia are complex because of large land surface heterogeneity, such as land cover, vegetation growth rates, soil types, and varying responses to climate variations. This makes accurately estimating NEE over Asia challenging. We believe this study is therefore useful to improve our understanding of the Asia regional terrestrial carbon cycle even though our estimation still has remaining uncertainties and biases in the inverted fluxes. By these comparisons, we can also conclude that our inferred Asia land surface CO_2 fluxes support a view that both large boreal and mid-latitude carbon sinks in Asia are balanced partly by a small tropical source. This would support the earlier suggestion that Asia is of key interest to better understand the global terrestrial carbon budget in the context of climate change.

The majority of the CO_2 sink was found in the areas dominated by forests, crops and grass/shrubs, although these were

not all individually constrained by the observations. Asian forests were estimated to be a large sink ($-0.77\,\mathrm{Pg\,C\,yr^{-1}}$) during the period 2006–2010, the sink size is slightly larger than the bottom-up derived results of Pan et al. (2011) ($-0.62\,\mathrm{Pg\,C\,yr^{-1}}$) for the period 1990–2007. One cause of this discrepancy is likely due to that our estimate is presented at a coarse resolution (a $1^\circ \times 1^\circ$ grid may contain other biomes with lower carbon uptake than forests). Another reason may be that about half of Temperate Eurasia was not included in the statistical analysis by Pan et al. (2011). Note that the carbon accumulation in wood products is not considered in our estimates and needs further analysis in future studies.

The croplands in Asia were identified to be an average sink of $-0.20\,\mathrm{Pg\,C\,yr^{-1}}$ during the period 2006–2010. The uptake in croplands is likely associated with agricultural technique and crop management. Different from other natural ecosystems, crop ecosystems are usually under intensive farming cultivation, with regular fertilizing and irrigation of the crops. This increases crop production, and in return leads to high residues and root to the soil, which increases the carbon sink in cropland (Chen et al., 2013). However, the accumulation of crop carbon in most crop ecosystems is relatively low, and agricultural areas are even considered not to contribute to a long-term net sink (Fang et al., 2007; Piao et al., 2009; Tian et al., 2011). This is because the carbon accumulation in the crop biomass is harvested at least once per year and released back as CO_2 to the atmosphere after consumption. We should note that our estimate in the crop sink is different from the results of "crop no contribution " (Piao et al., 2009). Our atmospheric inversion system can well capture the crop's strong CO_2 uptake during the growing season, but the atmosphere locally does not reflect the emission of the harvested crops, which normally have been transported laterally and is consumed elsewhere. This harvested product is likely released from a region with high population density and hard to detect against high fossil fuel emissions, whereas the estimated crop flux remains a large net CO_2 uptake over the period considered even though the crop flux into the soil is relatively small. Thus the croplands' sink in this study might be overestimated due to the absence of harvesting in our modeling system. This issue was also raised by Peters et al. (2007, 2010).

Grassland/Shrub ecosystems also play an important role in the global carbon cycle, accounting for about 20 % of total terrestrial production and could be a potential carbon sink in future (Scurlock and Hall, 1998). The grass/shrub lands in Asia absorbed a total of $-0.44\,\mathrm{Pg\,C\,yr^{-1}}$, accounting for about 25 % of the total Asian terrestrial CO_2 sink, which is close to the averaged global grassland sink percentage of 20 %. Compared to the bottom-up results that net ecosystem productivity was $10.18\,\mathrm{g\,C\,m^{-2}\,yr^{-1}}$ by Yu et al. (2013), our estimate of $34.32\,\mathrm{g\,C\,m^{-2}\,yr^{-1}}$ is much higher. This might be due to the fact that the areas in this study include shrubs, whereas other studies only consider grasslands.

The Supplement related to this article is available online at doi:10.5194/acp-14-5807-2014-supplement.

Acknowledgements. We wish to thank the Y. Niwa of Geochemical Research Department, Meteorological Research Institute, Tsukuba, Japan for providing many important comparable results and useful comments on this study. We kindly acknowledge all atmospheric data providers to the ObsPack version 1.0.2, and those that contribute their data to WDCGG. We are grateful to M. Ramonet of French RAMCES (Réseau Atmosphérique de Mesure des Composés à Effet de Serre), A. J. Gomez-Pelaez of Izaña Atmospheric Research Center (IARC), Meteorological State Agency of Spain (AEMET), Spain, B. Stephens of NCAR, L. Haszpra of Hungarian Meteorological Service and S. Hammer of University of Heidelberg, Institut fuer Umweltphysik for CO_2 time series used in this assimilation system. This research is supported by a research grant (2010CB950704) under the Global Change Program of the Chinese Ministry of Science and Technology, the Strategic Priority Research Program "Climate Change: Carbon Budget and Related Issues" of the Chinese Academy of Sciences (XDA05040403), the National High Technology Research and Development Program of China (Grant no. 2013AA122002),the research grant (41271116) funded by the National Science Foundation of China, a Research Plan of LREIS (O88RA900KA), CAS, a research grant (2012ZD010) of Key Project for the Strategic Science Plan in IGSNRR, CAS, and "One Hundred Talents" program funded by the Chinese Academy of Sciences. Wouter Peters was supported by an NWO VIDI Grant (864.08.012) and the Chinese-Dutch collaboration was funded by the China Exchange Program project (12CDP006). I. van der Laan-Luijkx has received funding from the European Union's Seventh Framework Programme (FP7/2007–2013) under grant agreement no. 283080, project GEOCARBON.

Edited by: R. Keeling

References

Baker, D., Law, R., Gurney, K., Rayner, P., Peylin, P., Denning, A., Bousquet, P., Bruhwiler, L., Chen, Y. H., and Ciais, P.: TransCom 3 inversion intercomparison: Impact of transport model errors on the interannual variability of regional CO_2 fluxes, 1988–2003, Global Biogeochem. Cy., 20, GB1002, doi:10.1029/2004GB002439, 2006.

Boden, T., Marland, G., and Andres, R.: Global, regional, and national fossil-fuel CO_2 emissions, Carbon Dioxide Information Analysis Center, Oak Ridge National Laboratory, US Department of Energy, Oak Ridge, Tenn., USA doi:10.3334/CDIAC/00001_V2011, 10, 2011.

Broquet, G., Chevallier, F., Bréon, F.-M., Kadygrov, N., Alemanno, M., Apadula, F., Hammer, S., Haszpra, L., Meinhardt, F., Morguí, J. A., Necki, J., Piacentino, S., Ramonet, M., Schmidt, M., Thompson, R. L., Vermeulen, A. T., Yver, C., and Ciais, P.: Regional inversion of CO_2 ecosystem fluxes from atmospheric measurements: reliability of the uncertainty estimates, Atmos. Chem. Phys., 13, 9039–9056, doi:10.5194/acp-13-9039-2013, 2013.

Cao, M., PRINCE, S. D., Li, K., TAO, B., SMALL, J., and Shao, X.: Response of terrestrial carbon uptake to climate interannual variability in China, Glob. Change Biol., 9, 536–546, 2003.

Chen, B., Chen, J. M., and Ju, W.: Remote sensing-based ecosystem-atmosphere simulation scheme (EASS)–Model formulation and test with multiple-year data, Ecol. Model., 209, 277–300, 2007.

Chen, B., Coops, N. C., Fu, D., Margolis, H. A., Amiro, B. D., Black, T. A., Arain, M. A., Barr, A. G., Bourque, C. P. A., and Flanagan, L. B.: Characterizing spatial representativeness of flux tower eddy-covariance measurements across the Canadian Carbon Program Network using remote sensing and footprint analysis, Remote Sens. Environ., 124, 742–755, 2012.

Chen, Z., Yu, G., Ge, J., Sun, X., Hirano, T., Saigusa, N., Wang, Q., Zhu, X., Zhang, Y., and Zhang, J.: Temperature and precipitation control of the spatial variation of terrestrial ecosystem carbon exchange in the Asian region, Agr. Forest Meteorol., 182–183, 266–276, 2013.

Chevallier, F. and O'Dell, C. W.: Error statistics of Bayesian CO_2 flux inversion schemes as seen from GOSAT, Geophys. Res. Lett., 40, 1252–1256, 2013.

Clark, D. A., Brown, S., Kicklighter, D. W., Chambers, J. Q., Thomlinson, J. R., and Ni, J.: Measuring net primary production in forests: concepts and field methods, Ecol. Appl., 11, 356–370, 2001.

Commission, E.: Joint Research Centre (JRC)/Netherlands Environmental Assessment Agency (PBL): Emission Database for Global Atmospheric Research (EDGAR), release version 4.0, 2009.

Deng, F., Chen, J. M., Ishizawa, M., YUEN, C. W. A. I., Mo, G., Higuchi, K., Chan, D., and Maksyutov, S.: Global monthly CO_2 flux inversion with a focus over North America, Tellus B, 59, 179–190, 2007.

Fan, Z. M., Li, J., and Yue, T. X.: Changes of Climate-Vegetation Ecosystem in Loess Plateau of China, Procedia Environmental Sciences, 13, 715–720, 2012.

Fang, J., Chen, A., Peng, C., Zhao, S., and Ci, L.: Changes in forest biomass carbon storage in China between 1949 and 1998, Science, 292, 2320, doi:10.1126/science.1058629, 2001.

Fang, J., Guo, Z., Piao, S., and Chen, A.: Terrestrial vegetation carbon sinks in China, 1981–2000, Sci. China Ser. D, 50, 1341–1350, 2007.

Francey, R. J., Trudinger, C. M., van der Schoot, M., Law, R. M., Krummel, P. B., Langenfelds, R. L., Steele, L. P., Allison, C. E., Stavert, A. R., and Andres, R. J.: Atmospheric verification of anthropogenic CO_2 emission trends, Nature Climate Change, 3, 520–524, 2013.

Friedl, M. A., McIver, D. K., Hodges, J. C., Zhang, X., Muchoney, D., Strahler, A. H., Woodcock, C. E., Gopal, S., Schneider, A., and Cooper, A.: Global land cover mapping from MODIS: algorithms and early results, Remote Sens. Environ., 83, 287–302, 2002.

Giglio, L., van der Werf, G. R., Randerson, J. T., Collatz, G. J., and Kasibhatla, P.: Global estimation of burned area using MODIS active fire observations, Atmos. Chem. Phys., 6, 957–974, doi:10.5194/acp-6-957-2006, 2006.

Gurney, K. R., Law, R. M., Denning, A. S., Rayner, P. J., Baker, D., Bousquet, P., Bruhwiler, L., Chen, Y. H., Ciais, P., and Fan, S.: Towards robust regional estimates of CO_2 sources and sinks using atmospheric transport models, Nature, 415, 626–630, 2002.

Gurney, K. R., Law, R. M., Denning, A. S., Rayner, P. J., Baker, D., Bousquet, P., Bruhwiler, L., CHEN, Y. H., Ciais, P., and Fan, S.: TransCom 3 CO_2 inversion intercomparison: 1. Annual mean control results and sensitivity to transport and prior flux information, Tellus B, 55, 555–579, 2003.

Gurney, K. R., Law, R. M., Denning, A. S., Rayner, P. J., Pak, B. C., Baker, D., Bousquet, P., Bruhwiler, L., Chen, Y. H., and Ciais, P.: Transcom 3 inversion intercomparison: Model mean results for the estimation of seasonal carbon sources and sinks, Global Biogeochem. Cy., 18, GB1010, doi:10.1029/2003GB002111, 2004.

Gurney, K. R., Baker, D., Rayner, P., and Denning, S.: Interannual variations in continental-scale net carbon exchange and sensitivity to observing networks estimated from atmospheric CO_2 inversions for the period 1980 to 2005, Global Biogeochem. Cy., 22, GB3025, doi:10.1029/2007GB003082, 2008.

Hayes, D. J., McGuire, A. D., Kicklighter, D. W., Gurney, K. R., Burnside, T., and Melillo, J. M.: Is the northern high-latitude land-based CO_2 sink weakening?, Global Biogeochem. Cy., 25, GB3018, doi:10.1029/2010GB003813, 2011.

Houghton, R.: Balancing the global carbon budget, Annu. Rev. Earth Pl. Sc., 35, 313–347, 2007.

Huber, M. and Knutti, R.: Anthropogenic and natural warming inferred from changes in Earth's energy balance, Nat. Geosci., 5, 31–36, 2011.

Ichii, K., Kondo, M., Lee, Y.-H., Wang, S.-Q., Kim, J., Ueyama, M., Lim, H.-J., Shi, H., Suzuki, T., and Ito, A.: Site-level model–data synthesis of terrestrial carbon fluxes in the CarboEastAsia eddy-covariance observation network: toward future modeling efforts, J. For. Res., 18, 13–20, 2013.

Ito, A.: The regional carbon budget of East Asia simulated with a terrestrial ecosystem model and validated using AsiaFlux data, Agr. Forest Meteorol., 148, 738–747, 2008.

Jacobson, A. R., Mikaloff Fletcher, S. E., Gruber, N., Sarmiento, J. L., and Gloor, M.: A joint atmosphere-ocean inversion for surface fluxes of carbon dioxide: 1. methods and global-scale fluxes, Global Biogeochem. Cy., 21, GB1020, doi:10.1029/2006GB002703, 2007.

Jiang, F., Wang, H. W., Chen, J. M., Zhou, L. X., Ju, W. M., Ding, A. J., Liu, L. X., and Peters, W.: Nested atmospheric inversion for the terrestrial carbon sources and sinks in China, Biogeosciences, 10, 5311–5324, doi:10.5194/bg-10-5311-2013, 2013.

Krol, M., Houweling, S., Bregman, B., van den Broek, M., Segers, A., van Velthoven, P., Peters, W., Dentener, F., and Bergamaschi, P.: The two-way nested global chemistry-transport zoom model TM5: algorithm and applications, Atmos. Chem. Phys., 5, 417–432, doi:10.5194/acp-5-417-2005, 2005.

Le Quere, C., Raupach, M. R., Canadell, J. G., Marland, G., Bopp, L., Ciais, P., Conway, T. J., Doney, S. C., Feely, R. A., Foster, P., Friedlingstein, P., Gurney, K., Houghton, R. A., House, J. I., Huntingford, C., Levy ,P. E., Lomas, M. R., Majkut, J., Metzl, N., Ometto, J. P., Peters, G. P., Prentice, I. C., Randerson, J. T., Running, S. W., Sarmiento, J. L., Schuster1, U., Sitch, S., Takahashi, T., Viovy, N., van der Werf, G. R., and Woodward, F. I.: Trends in the sources and sinks of carbon dioxide, Nat. Geosci., 2, 831–836, 2009.

Machida, T., Matsueda, H., Sawa, Y., Nakagawa, Y., Hirotani, K., Kondo, N., Goto, K., Nakazawa, T., Ishikawa, K., and Ogawa, T.:

Worldwide measurements of atmospheric CO_2 and other trace gas species using commercial airlines, J. Atmos. Ocean. Tech., 25, 1744–1754, 2008.

Machida, T., Tohjima, Y., Katsumata, K., and Mukai, H.: A new CO_2 calibration scale based on gravimetric one-step dilution cylinders in National Institute for Environmental Studies-NIES 09 CO_2 scale, World Meteorol. Organ., Geneva, Switzerland, 114–119, 2011.

Maki, T., Ikegami, M., Fujita, T., Hirahara, T., Yamada, K., Mori, K., Takeuchi, A., Tsutsumi, Y., Suda, K., and Conway, T.: New technique to analyse global distributions of CO_2 concentrations and fluxes from non-processed observational data, Tellus B, 62, 797–809, 2010.

Maksyutov, S., Machida, T., Mukai, H., Patra, P. K., Nakazawa, T., and Inoue, G.: Effect of recent observations on Asian CO_2 flux estimates by transport model inversions, Tellus B, 55, 522–529, 2003.

Marland, G., Boden, T. A., Andres, R. J., Brenkert, A., and Johnston, C.: Global, Regional, and National Fossil Fuel CO_2 Emissions, Trends: a Compendium of Data on Global Change, Carbon Dioxide Information Analysis Center, Oak Ridge National Laboratory, http://cdiac.ornl.gov/trends/emis/overview (last access: 1 May 2007), 2003.

Masarie, K., Pétron, G., Andrews, A., Bruhwiler, L., Conway, T., Jacobson, A., Miller, J., Tans, P., Worthy, D., and Peters, W.: Impact of CO_2 measurement bias on CarbonTracker surface flux estimates, J. Geophys. Res., 116, D17305, doi:10.1029/2011JD016270, 2011.

Matsueda, H., Machida, T., Sawa, Y., Nakagawa, Y., Hirotani, K., Ikeda, H., Kondo, N., and Goto, K.: Evaluation of atmospheric CO sub (2) measurements from new flask air sampling of JAL airliner observations, Pap. Meteorol. Geophys., 59, 1–17, 2008.

Mizoguchi, Y., Miyata, A., Ohtani, Y., Hirata, R., and Yuta, S.: A review of tower flux observation sites in Asia, J. For. Res., 14, 1–9, 2009.

Mohammat, A., Wang, X., Xu, X., Peng, L., Yang, Y., Zhang, X., Myneni, R. B., and Piao, S.: Drought and spring cooling induced recent decrease in vegetation growth in Inner Asia, Agr. Forest Meteorol., 178–179, 21–30, 2012.

NationalClimateCenter: 2010 China Climate Bulletin, China Meteorological Press, 1, 34 pp., 2011.

Niwa, Y., Patra, P. K., Sawa, Y., Machida, T., Matsueda, H., Belikov, D., Maki, T., Ikegami, M., Imasu, R., Maksyutov, S., Oda, T., Satoh, M., and Takigawa, M.: Three-dimensional variations of atmospheric CO_2: aircraft measurements and multi-transport model simulations, Atmos. Chem. Phys., 11, 13359–13375, doi:10.5194/acp-11-13359-2011, 2011.

Niwa, Y., Machida, T., Sawa, Y., Matsueda, H., Schuck, T. J., Brenninkmeijer, C. A. M., Imasu, R., and Satoh, M.: Imposing strong constraints on tropical terrestrial CO_2 fluxes using passenger aircraft based measurements, J. Geophys. Res.-Atmos., 117, D11303, doi::10.1029/2012JD01747, 2012.

Oikawa, T. and Ito, A.: Modeling carbon dynamics of terrestrial ecosystems in monsoon Asia, Present and future modeling global environmental change: toward integrated modeling, TERRAPUB, Tokyo, 207–219, 2001.

Olivier, J. and Berdowski, J.: Global Emission Sources and Sinks, Lisse, the Netherlands, Balkema, 2001.

Olson, J. S., Watts, J. A., and Allison, L. J.: Major World Ecosystem Complexes Ranked by Carbon in Live Vegetation: A Database, NDP-017, Oak Ridge Lab., Oak Ridge, Tenn, 1985.

Pan, Y., Birdsey, R. A., Fang, J., Houghton, R., Kauppi, P. E., Kurz, W. A., Phillips, O. L., Shvidenko, A., Lewis, S. L., Canadell, J. G., Ciais, P., Jackson, R. B., Pacala, S. W., McGuire, A. D., Piao, S., Rautiainen, A., Sitch, S., and Hayes, D.: A Large and Persistent Carbon Sink in the World's Forests, Science, 333, 988–993, 2011.

Patra, P. K., Niwa, Y., Schuck, T. J., Brenninkmeijer, C. A. M., Machida, T., Matsueda, H., and Sawa, Y.: Carbon balance of South Asia constrained by passenger aircraft CO_2 measurements, Atmos. Chem. Phys., 11, 4163–4175, doi:10.5194/acp-11-4163-2011, 2011.

Patra, P. K., Canadell, J. G., and Lal, S.: The rapidly changing greenhouse gas budget of Asia, Eos, Transactions American Geophysical Union, 93, 237–237, 2012.

Patra, P. K., Canadell, J. G., Houghton, R. A., Piao, S. L., Oh, N.-H., Ciais, P., Manjunath, K. R., Chhabra, A., Wang, T., Bhattacharya, T., Bousquet, P., Hartman, J., Ito, A., Mayorga, E., Niwa, Y., Raymond, P. A., Sarma, V. V. S. S., and Lasco, R.: The carbon budget of South Asia, Biogeosciences, 10, 513–527, doi:10.5194/bg-10-513-2013, 2013.

Peters, G. P., Marland, G., Le Quéré, C., Boden, T., Canadell, J. G., and Raupach, M. R.: Rapid growth in CO_2 emissions after the 2008-2009 global financial crisis, Nature Climate Change, 2, 2–4, 2011.

Peters, W., Jacobson, A. R., Sweeney, C., Andrews, A. E., Conway, T. J., Masarie, K., Miller, J. B., Bruhwiler, L. M. P., Petron, G., and Hirsch, A. I.: An atmospheric perspective on North American carbon dioxide exchange: CarbonTracker, P. Natl. Acad. Sci. USA, 104, 18925–18930, 2007.

Peters, W., Krol, M., Van der Werf, G., Houweling, S., Jones, C., Hughes, J., Schaefer, K., Masarie, K., Jacobson, A., and Miller, J.: Seven years of recent European net terrestrial carbon dioxide exchange constrained by atmospheric observations, Glob. Change Biol., 16, 1317–1337, 2010.

Peylin, P., Rayner, P. J., Bousquet, P., Carouge, C., Hourdin, F., Heinrich, P., Ciais, P., and AEROCARB contributors: Daily CO_2 flux estimates over Europe from continuous atmospheric measurements: 1, inverse methodology, Atmos. Chem. Phys., 5, 3173–3186, doi:10.5194/acp-5-3173-2005, 2005.

Peylin, P., Law, R. M., Gurney, K. R., Chevallier, F., Jacobson, A. R., Maki, T., Niwa, Y., Patra, P. K., Peters, W., Rayner, P. J., Rödenbeck, C., van der Laan-Luijkx, I. T., and Zhang, X.: Global atmospheric carbon budget: results from an ensemble of atmospheric CO_2 inversions, Biogeosciences, 10, 6699–6720, doi:10.5194/bg-10-6699-2013, 2013.

Piao, S., Fang, J., Ciais, P., Peylin, P., Huang, Y., Sitch, S., and Wang, T.: The carbon balance of terrestrial ecosystems in China, Nature, 458, 1009–1013, 2009.

Piao, S. L., Ciais, P., Lomas, M., Beer, C., Liu, H. Y., Fang, J. Y., Friedlingstein, P., Huang, Y., Muraoka, H., Son, Y. H., and Woodward, I.: Contribution of climate change and rising CO(2) to terrestrial carbon balance in East Asia: A multi-model analysis, Global Planet. Change, 75, 133–142, 2011.

Piao, S. L., Ito, A., Li, S. G., Huang, Y., Ciais, P., Wang, X. H., Peng, S. S., Nan, H. J., Zhao, C., Ahlström, A., Andres, R. J., Chevallier, F., Fang, J. Y., Hartmann, J., Huntingford, C., Jeong,

S., Levis, S., Levy, P. E., Li, J. S., Lomas, M. R., Mao, J. F., Mayorga, E., Mohammat, A., Muraoka, H., Peng, C. H., Peylin, P., Poulter, B., Shen, Z. H., Shi, X., Sitch, S., Tao, S., Tian, H. Q., Wu, X. P., Xu, M., Yu, G. R., Viovy, N., Zaehle, S., Zeng, N., and Zhu, B.: The carbon budget of terrestrial ecosystems in East Asia over the last two decades, Biogeosciences, 9, 3571–3586, doi:10.5194/bg-9-3571-2012, 2012.

Randall, D. A., Dazlich, D. A., Zhang, C., Denning, A. S., Sellers, P. J., Tucker, C. J., Bounoua, L., Los, S. O., Justice, C. O., and Fung, I.: A revised land surface parameterization (SiB2) for GCMs. 3. The greening of the Colorado State University general circulation model, J. Climate, 9, 738–763, 1996.

Randerson, J. T., Thompson, M. V., Conway, T. J., Fung, I. Y., and Field, C. B.: The contribution of terrestrial sources and sinks to trends in the seasonal cycle of atmospheric carbon dioxide, Global Biogeochem. Cy., 11, 535–560, 1997.

Raupach, M. R., Marland, G., Ciais, P., Le Quéré, C., Canadell, J. G., Klepper, G., and Field, C. B.: Global and regional drivers of accelerating CO_2 emissions, P. Natl. Acad. Sci. USA, 104, 10288–10293, 2007.

Richardson, A. D., Hollinger, D. Y., Dail, D. B., Lee, J. T., Munger, J. W., and O'keefe, J.: Influence of spring phenology on seasonal and annual carbon balance in two contrasting New England forests, Tree Physiol., 29, 321–331, 2009.

Rivier, L., Peylin, P., Ciais, P., Gloor, M., Rödenbeck, C., Geels, C., Karstens, U., Bousquet, P., Brandt, J., and Heimann, M.: European CO_2 fluxes from atmospheric inversions using regional and global transport models, Clim. Change, 103, 93–115, 2010.

Rivier, L., Peylin, P., Ciais, P., Gloor, M., Rödenbeck, C., Geels, C., Karstens, U., Bousquet, P., Brandt, J., and Heimann, M.: European CO_2 fluxes from atmospheric inversions using regional and global transport models, in: Greenhouse Gas Inventories, Springer, 2011.

Saeki, T., Maksyutov, S., Sasakawa, M., Machida, T., Arshinov, M., Tans, P., Conway, T., Saito, M., Valsala, V., and Oda, T.: Carbon flux estimation for Siberia by inverse modeling constrained by aircraft and tower CO_2 measurements, J. Geophys. Res.-Atmos., 118, 1100–1122, 2013

Sawa, Y., Machida, T., and Matsueda, H.: Seasonal variations of CO_2 near the tropopause observed by commercial aircraft, J. Geophys. Res., 113, D23301, doi:10.1029/2008JD010568, 2008.

Scurlock, J. and Hall, D.: The global carbon sink: a grassland perspective, Glob. Change Biol., 4, 229–233, 1998.

Sellers, P., Mintz, Y., Sud, Y., and Dalcher, A.: A simple biosphere model (SiB) for use within general circulation models, J. Atmos. Sci., 43, 505–531, 1986.

Sellers, P., Randall, D., Collatz, G., Berry, J., Field, C., Dazlich, D., Zhang, C., Collelo, G., and Bounoua, L.: A revised land surface parameterization (SiB2) for atmospheric GCMs. Part I: Model formulation, J. Climate, 9, 676–705, 1996.

Stephens, B. B., Gurney, K. R., Tans, P. P., Sweeney, C., Peters, W., Bruhwiler, L., Ciais, P., Ramonet, M., Bousquet, P., and Nakazawa, T.: Weak northern and strong tropical land carbon uptake from vertical profiles of atmospheric CO_2, Science, 316, 1732–1735, 2007.

Takahashi, T., Wanninkhof, R., Feely, R., Weiss, R., Chipman, D., Bates, N., Olafsson, J., Sabine, C., and Sutherland, S.: Net Sea-Air CO_2 Flux Over the Global Oceans: an Improved Estimate Based on the Sea-Air pCO_2 Difference, Proceedings of the 2nd International Symposium CO_2 in the Oceans, Tsukuba, Japan: National Institute for Environmental Studies, 1999.

Thoning, K. W., Tans, P. P., and Komhyr, W. D.: Atmospheric carbon dioxide at Mauna Loa Observatory: 2. Analysis of the NOAA GMCC data, 1974–1985, J. Geophys. Res.-Atmos., 94, 8549–8565, 1989.

Tian, H., Melillo, J., Lu, C., Kicklighter, D., Liu, M., Ren, W., Xu, X., Chen, G., Zhang, C., and Pan, S.: China's terrestrial carbon balance: Contributions from multiple global change factors, Global Biogeochem. Cy., 25, GB1007, doi:10.1029/2010GB003838, 2011.

Walther, G.-R., Post, E., Convey, P., Menzel, A., Parmesan, C., Beebee, T. J., Fromentin, J.-M., Hoegh-Guldberg, O., and Bairlein, F.: Ecological responses to recent climate change, Nature, 416, 389–395, 2002.

Wang, H., Zhang, R., Liu, M., and Bi, J.: The carbon emissions of Chinese cities, Atmos. Chem. Phys., 12, 6197–6206, doi:10.5194/acp-12-6197-2012, 2012.

Wang, X., Piao, S., Ciais, P., Li, J., Friedlingstein, P., Koven, C., and Chen, A.: Spring temperature change and its implication in the change of vegetation growth in North America from 1982 to 2006, P. Natl. Acad. Sci., 108, 1240–1245, 2011.

van der Werf, G. R., Randerson, J. T., Giglio, L., Collatz, G. J., Kasibhatla, P. S., and Arellano Jr., A. F.: Interannual variability in global biomass burning emissions from 1997 to 2004, Atmos. Chem. Phys., 6, 3423–3441, doi:10.5194/acp-6-3423-2006, 2006.

Yang, Z., Washenfelder, R., Keppel-Aleks, G., Krakauer, N., Randerson, J., Tans, P., Sweeney, C., and Wennberg, P.: New constraints on Northern Hemisphere growing season net flux, Geophys. Res. Lett., 34, L12807, doi:10.1029/2007GL029742, 2007.

Yu, G. R., Zhu, X. J., Fu, Y. L., He, H. L., Wang, Q. F., Wen, X. F., Li, X. R., Zhang, L. M., Zhang, L., and Su, W.: Spatial patterns and climate drivers of carbon fluxes in terrestrial ecosystems of China, Glob. Change Biol., 19, 798–810, 2013.